Development of a 5-Component Gasoline Surrogate Model Using Recent Advancements in the Detailed $H_2/O_2/CO/C_1$-C_3 Mechanism for Decoupling Methodology

Shiyou Yang[a,*], **Quande Wang**[b], **Henry J. Curran**[b], and **Ming Jia**[c]

[a] Research and Advanced Engineering, Ford Motor Company, 2101 Village Road, Dearborn, Michigan 48124, USA. Email: syang33@ford.com

[b] Combustion Chemistry Centre, School of Chemistry, Ryan Institute, National University of Ireland Galway, University Road, Galway, H91 TK33, Ireland

[c] School of Energy and Power Engineering, Dalian University of Technology, Dalian 116024, China

ABSTRACT

In the present work, a 5-component gasoline surrogate chemical kinetic mechanism has been developed and validated. The first novelty of this mechanism is that a recently advanced $H_2/O_2/CO/C_1$ detailed sub-mechanism is adopted for accurately predicting the laminar flame speeds over a wide range of operating conditions and a recently advanced C_2–C_3 detailed sub-mechanism is used due to its potential benefits on accurate flame propagation simulation in order to overcome the drawbacks in the original decoupling methodology. The second novelty of this mechanism is that the sub-mechanisms of propyne and allene which are important for soot formation from non-aromatics have been improved significantly. For each of the five gasoline surrogate components (iso-octane, *n*-heptane, iso-hexane, 1-hexene, and toluene) a skeletal sub-mechanism, which determines the simulation of ignition delay times, is constructed for species C_4–C_n. The five skeletal sub-mechanisms are coupled with the new C_2–C_3 and $H_2/O_2/CO/C_1$ detailed sub-mechanisms. Together with a reduced NOx (oxides of nitrogen) sub-mechanism, the 5-component gasoline surrogate chemical kinetic mechanism has 214 species and 1233 reactions, which are feasible currently for CFD simulation of gasoline engine combustion, emissions, and knock. The new $H_2/O_2/CO/C_1$ and C_2-C_3 detailed sub-mechanisms were

validated with selected experimental data of ignition delay times, laminar flame speeds, and important species profiles in the literature. The reaction rate constants of the five skeletal sub-mechanisms were optimized in this work to match available experimental data of either pure fuels or fuel blends, including real gasoline fuels. The validation results show that the prediction accuracy of the 5-component gasoline surrogate chemical kinetic mechanism of the present work can be less than 5% for various fuel blends under a pressure range of 1.0~80.0 bar, a temperature range of 300~1260 K, and an equivalence ratio range of 0.5~2.5.

KEYWORDS: CHEMICAL KINETIC MECHANISM; GASOLINE SURROGATE; MULTI-COMPONENT FUEL

1. INTRODUCTION

Higher efficiency and lower unburned hydrocarbon (UHC) emissions are two major requirements for future gasoline engines to alleviate the pressure of limited petroleum storage in the world as well as to meet the stringent regulations of emissions. To meet these requirements, researchers have been studying several advanced combustion concepts for internal combustion engines in the past 20 years, such like Homogeneous Charge Compression Ignition (HCCI) [1], Pre-mixed Charge Compression Ignition (PCCI) [2], Reactivity Controlled Compression Ignition (RCCI) [3], and Gasoline Direct Injection (GDI) [4] which has already been applied to the automobile market. In recent years, a new combustion concept–Gasoline Compression Ignition (GCI), has been investigated by some researchers for its further potential on improving fuel economy and reducing pollutant emissions [5]. In the research and development of these new engine combustion concepts, multi-dimensional computational fluid dynamics (CFD) has played a very important role. In CFD combustion simulation, to accurately predict autoignition, flame propagation, and emissions characteristics of engines, an accurate chemical kinetic mechanism for hydrocarbons and diverse surrogate fuels is an indispensable prerequisite. However, since commercial gasoline fuel generally contains hundreds of individual components, it is still impossible to construct a detailed chemical kinetic mechanism consisting of all the components of real

gasoline fuel and then apply the mechanism directly to engine combustion simulation using multidimensional CFD due to the limitations of available computational resources. It has been accepted that a surrogate gasoline fuel with several components can capture certain combustion behaviors of a target fuel containing many components so that a mechanism with a suitable size is possible for engine CFD application.

Because of its comparable octane number with gasoline fuel, iso-octane has been widely used by some researchers as a single-component surrogate for gasoline to simulate the flame propagation of gasoline engines. Primary reference fuel (PRF), which is obtained from a mixture of *n*-heptane and iso-octane and has an octane number from 0 to 100, has also been widely used by some researchers as a model fuel of gasoline (e.g., Selim et al. [6]). However, both the iso-octane and PRF mechanisms cannot well describe the oxidation processes of those major chemical components existing in real gasoline fuel, which lead to different behaviors of ignition and flame propagation. Moreover, pollutant emissions with iso-octane and *n*-heptane also differ from those of gasoline fuel. Especially, due to the lack of aromatic compounds, iso-octane and *n*-heptane produce different soot emissions than gasoline fuel. To overcome the limitations of a one-component or a two-component surrogate, ternary and more complex blends have been proposed as gasoline surrogate fuels in recent years. For example, Wang et al. [7] proposed a TRF (toluene reference fuel) including *n*-heptane, iso-octane and toluene for gasoline surrogate fuel. The proposed surrogate composition along with their reduced mechanism were capable of capturing combustion and emissions in HCCI and DICI (direct injection compression ignition) engine simulations. Based on Wang et al.'s work [7], Liu et al. [8] constructed an improved TRF-2,5-dimethylfuran (DMF25)-PAH (polycyclic aromatic hydrocarbon) combustion mechanism. A four-component mixture including *n*-heptane, iso-octane, toluene and a C_5-C_6 olefin has been used as a gasoline surrogate fuel by Mehl et al. [9]. This gasoline surrogate composition coupled with an LLNL (Lawrence Livermore National Laboratory) chemical kinetic mechanism [9] was successfully applied to the simulation of an HCCI engine under naturally aspirated and boosted conditions. Puduppakkam et al. [10] constructed a 5-component gasoline

surrogate fuel containing *n*-heptane, iso-octane, iso-hexane, 1-hexene and toluene by using a program called surrogate blend optimizer. Based on a master kinetic mechanism, which has 2099 species and 9789 elementary reactions, a final reduced mechanism with 425 species and 3128 reactions was achieved for RCCI conditions. Although the reduced mechanism is still too complex for the application to practical 3D gasoline engine simulations, after two advanced chemistry solution techniques including dynamic cell clustering (DCC) and sparse chemistry solver were employed the computational time could be reasonably shortened [10].

Even a gasoline surrogate model with several components is used for real gasoline fuel, the integration of detailed mechanisms of the surrogate components into multi-dimensional CFD models for engines still leads to extremely long computational times. Therefore, skeletal or reduced mechanisms that can shorten the computational time while maintaining necessary accuracy are of great interests for 3D simulations of gasoline engines. One popular method to reduce a detailed mechanism is the DRG (direct relation graph) automatic mechanism reduction method proposed by Lu et al. [11]. Based on the DRG method, the DRGEP (direct relation graph with error propagation) mechanism reduction method was developed by Pepiot-Desjardins et al. [12]. Using the DRGEP and sensitivity analysis followed by a further unimportant reaction elimination method, Niemeyer and Sung [13] presented recommendations for performing mechanism reduction for multicomponent surrogates. Stagni et al. [14] also proposed an automatic mechanism reduction approach based on a species-targeted sensitivity analysis strategy. Using the DRGEP-based approach, Chen et al. [15] developed a reduced chemical kinetic mechanism for a Haltermann 437 certification gasoline fuel and applied the mechanism to the simulation of a GCI engine. This mechanism was reduced only using ignition delay time as the target parameter. However, it has been found by Mehl et al. [16] that a reduced mechanism only based on auto ignition characteristics cannot give accurate predictions of laminar flame speeds, which are very important for turbulent pre-mixed gasoline engine combustion modeling. Another method to develop a mechanism with a smaller size is to use the decoupling methodology proposed by Liu et al. [17], which is of interests by some researchers in

recent years. Liu et al. found that the prediction of flame propagation is dominated by small species (radicals and molecules) and decoupled from the low-temperature chemistry, while the ignition characteristics depend on both the smaller molecular fragments and low-temperature chemistry. Based on their analysis, the decoupling methodology considers the combustion process of a fuel as two parts: one part is ignition, which is largely dependent on the specific fuel, and the other part is flame propagating after ignition, which is mainly controlled by reactions involving small radicals and molecules of CO–C_1 and is less dependent on the specific fuel. Therefore, using the decoupling methodology a reduced mechanism can be constructed with a comprehensive part to describe the detailed reaction processes of CO–C_1 radical and molecules as the 'core' as well as a skeletal part that couples the 'core' to control the ignition characteristics. In Liu et al.'s work [17, 18] the decoupling methodology was used to develop a skeletal chemical kinetic mechanism for iso-octane with 32 species and 111 reactions, as well as a skeletal chemical kinetic mechanism for primary reference fuel with 41 species and 124 reactions. Their results showed that both the iso-octane mechanism and PRF mechanism are well promising for various reactors and engine applications incorporated with multidimensional CFD modeling. Yang et al. [19] improved the mechanisms from Liu et al's work using laminar flame speeds for practical engine operating conditions, and successfully applied the improved mechanism to the simulation of gasoline engine combustion and emissions with very good agreements to experimental data. Using the same methodology, Liu et al. [20] expanded their PRF mechanism to include toluene as a component of gasoline surrogate model and achieved good results. Chang et al. [21] built a diesel surrogate model by considering *n*-decane, iso-octane, MCH (methylcyclohexane) and toluene using the decoupling methodology. The mechanism was validated against experimental data of ignition delay times in shock tubes, species concentrations in jet-stirred and flow reactors, and laminar flame speeds over some operating ranges.

In the mechanisms of Liu et al [17, 18, 20], Yang et al. [19] and Chang et al. [21], the 'core' part CO–C_1 sub-mechanism is from Klippenstein et al. [22] and Li et al. [23] for the ignition of methanol at high

pressure by using the *ab initio* transition state theory, and the transition part C_2–C_3 sub-mechanism including six species (C_2H_3, C_2H_4, C_3H_4, C_3H_5, C_3H_6, and C_3H_7) is from the model of Patel et al. [24] because of its small size. Recently, Kéromnès et al. [25], Metcalfe et al. [26], and Burke et al. [27] have updated H_2/O_2/CO/C_1 detailed sub-mechanism to characterize the kinetic and thermochemical properties of a large number of CO–C_1 based hydrocarbons and oxygenated fuels over a wide range of experimental conditions. The C_2–C_3 sub-mechanism used in the model of Patel et al. [24] is practical due to its simplicity, but some researchers [21] believe that it may affect the accuracy of laminar flame speed simulation over some conditions. Metcalfe et al. [26] and Burke et al. [28, 29] have developed a detailed C_2–C_3 sub-mechanism which is constructed in a hierarchical way for larger C_2–C_3 carbon species such as ethane, ethylene, acetylene, allene, propyne, and propene, as well as oxygenated species. The new C_2–C_3 sub-mechanism has been validated against a large array of experimental measurements including data from shock tubes, rapid compression machines, flames, jet-stirred and plug-flow reactors. In Kéromnès et al.'s work [25], they found that the reaction sequence $H_2 + H\dot{O}_2 \leftrightarrow \dot{H} + H_2O_2$ followed by $H_2O_2\,(+M) \leftrightarrow \dot{O}H + \dot{O}H\,(+M)$ play a key role in hydrogen ignition under high-pressure and intermediate-temperature conditions and recommended a new reaction rate constant for this reaction based on available literature values and on their own mechanism validation. In Metcalfe et al.'s work [26], they developed a detailed chemical kinetic mechanism to describe the oxidation of C_1–C_2 hydrocarbon species, and validated the mechanism over a wide range of initial conditions. In their work, the performance of all the reactions and their interactions has been studied, and they avoided optimization of rate constants as far as possible, using experimentally measured values or high-level theoretically calculated values from the literature. In Burke et al.'s work [28, 29], they developed a detailed chemical kinetic mechanism to describe the combustion of propene under some experimental conditions. They highlighted some important reactions via flux and sensitivity analyses including: hydrogen atom abstraction from propene by molecular oxygen, hydroxyl, and hydroperoxyl radicals; allyl–allyl radical recombination; the reaction between allyl and hydroperoxyl

radicals; and the reactions of 1- and 2-propenyl radicals with molecular oxygen. In 2020, National University of Ireland Galway had the latest updates and improvements on the $H_2/O_2/CO/C_1$ and C_2–C_3 detailed sub-mechanisms, which will be briefly introduced in Section 2.

The aim of this study is to develop a gasoline multi-component chemical kinetic mechanism with a medium size which is feasible for gasoline engine 3D combustion modeling, while maintains higher accuracy. To achieve this aim, a gasoline surrogate model is first proposed by including iso-octane, iso-hexane, *n*-heptane, 1-hexene, and toluene, which represents the iso-paraffins, *n*-paraffins, olefins and aromatic hydrocarbons in real gasoline fuel, respectively. Then five skeletal oxidation mechanisms are constructed and optimized for the five gasoline surrogate components. The five skeletal sub-mechanisms are coupled with the above mentioned recently advanced C_2–C_3 and $H_2/O_2/CO/C_1$ detailed sub-mechanisms to generate an integrated mechanism. Extensive validations of the $H_2/O_2/CO/C_1$ and C_2–C_3 detailed sub-mechanisms, as well as the five skeletal sub-mechanisms are conducted, using experimental data of either a single component fuel or various fuel mixtures including gasoline fuel mixtures in various fundamental experiments under wide ranges of operating conditions.

2. CHEMICAL KINETIC MODEL DESCRIPTION

2.1 Gasoline Surrogate Components and Chemical Kinetic Mechanism Overall Structure

Since the constitute of gasoline fuel is highly variable, this work will mainly focus on a specific gasoline fuel whose name is Ford 98-RON-50E. Based on a breakdown of the chemical components in Ford 98-RON-50E gasoline fuel, the major categories of components are iso-alkanes, aromatics, olefins, and *n*-alkanes. Iso-alkanes class is a major constituent of the gasoline fuel (~40% by volume), in which iso-octane and iso-hexane make up the two major parts. In the gasoline surrogate model of this work, iso-octane (iC_8H_{18}) and iso-hexane (iC_6H_{14}) are selected as two surrogate components to represent the iso-alkanes class. Aromatics class is the second largest constituent of the gasoline fuel (~30% by volume). Most researchers [7, 8, 9, 10] think that toluene is a representative component of this class. In the model of this work, toluene ($C_6H_5CH_3$) is selected as

a surrogate component to represent the aromatics class. As recommended by Puduppakkam et al. [10], 1-hexene (C_6H_{12}-1) is selected as a surrogate component to represent the *n*-alkenes (olefins) class in this work. Also based on the breakdown of the chemical components in Ford 98-RON-50E gasoline fuel, *n*-heptane makes up the major portion of *n*-alkanes class. In this work, *n*-heptane (nC_7H_{16}) is selected as a surrogate component to represent the *n*-alkanes class. Relative to above four chemical classes, cycloalkanes only make up a small portion of the gasoline fuel, and hence will not be considered in the gasoline surrogate model of this work. The above choice of representative components for each hydrocarbon class is also based on the availability of kinetic models and experimental data for these components. After identification of components in the gasoline surrogate model, it is important to determine the proportion of each component. A program called Surrogate Blend Optimizer [10] was used to obtain the proportions of those surrogate components. In the surrogate blend optimization, appropriate model-fuel components are selected from a palette of options. Then, based on several fuel-property targets, the optimum model-fuel blend can be determined.

Table 1. Ford 98-RON-50E gasoline fuel surrogate blend optimization results

Model fuel components	Representing chemical class	Liquid % (mass)	Liquid % (volume)
iso-Octane (iC_8H_{18})	iso-Alkanes	37.0	39.91
iso-Hexane (iC_6H_{14})	iso-Alkanes	8.39	9.31
Toluene ($C_6H_5CH_3$)	Aromatics	40.0	34.51
1-Hexene (C_6H_{12}-1)	Alkenes	8.21	9.28
n-Heptane (nC_7H_{16})	*n*-Alkanes	6.4	6.99

Table 1 shows the surrogate blend optimization results for Ford 98-RON-50E gasoline fuel. With these proportions of the five components, Table 2 compares some properties between mean target of the gasoline fuel

and calculation of the surrogate model, including LHV (lower heating value), RON (research octane number), MON (motor octane number), sensitivity (RON–MON), molar H/C ratio, liquid density, and T50. From the comparison shown in Table 2 it can be seen that the surrogate model has satisfactory agreements with the mean target of the gasoline fuel for some major physical and chemical properties.

Table 2. Properties comparison between mean target and surrogate model

Property name	Mean target	Surrogate model
LHV (Lower Heating Value)	43.15 MJ/kg	43.13 MJ/kg
RON (Research Octane Number)	97.2	95.82
MON (Motor Octane Number)	88.6	90.47
Sensitivity (=RON-MON)	8.6	5.35
Molar H/C ratio	1.841	1.7745
Liquid density	743.4 kg/m^3	743.7 kg/m^3
T50 (temperature of 50% volume evaporated)	377.93 K	372.1 K

The reaction paths of the 5-component gasoline surrogate chemical kinetic mechanism developed in the present study are summarized in Figure 1. As can be seen, the mechanism is constructed by integrating the five skeletal sub-mechanisms for iso-octane (iC_8H_{18}), *n*-heptane (nC_7H_{16}), iso-hexane (iC_6H_{14}), 1-hexene (C_6H_{12}-1), and toluene ($C_6H_5CH_3$) with the recently advanced C_2–C_3 and $H_2/O_2/CO/C_1$ detailed sub-mechanisms. As mentioned earlier, the recently advanced $H_2/O_2/CO/C_1$ detailed sub-mechanism is mainly taken from the work of Kéromnès et al. [25], Metcalfe et al. [26], Burke et al. [27], and the latest advancements of National University of Ireland Galway in 2020 which will be described below, while the recently advanced C_2–C_3 detailed sub-mechanism is mainly taken from the work of Metcalfe et al. [26], Burke et al. [28, 29], and again the latest advancements of NUI-Galway in 2020. In the following sub-sections 2.2, 2.3, and 2.4, the new

characteristics of the recently advanced $H_2/O_2/CO/C_1–C_3$ detailed sub-mechanisms are summarized for readability of the paper. The reaction pathways for each of the five skeletal sub-mechanisms are described in the following sub-sections 2.5, 2.6, and 2.7. In this work the final mechanism is named as 'MCCh v2.0'. It must be pointed out that the decoupling methodology used in the present study may have some limitations. Comandini et al. [30] found that the flame speed of aromatics is also strongly affected by the ring chemistry, especially by the reactions involving the radicals of phenoxy, benzyl, and phenyl. An in-depth understanding of the chemistry of the investigated fuel in this work may be needed in the near future. It must also be mentioned that the co-oxidation or cross reactions for direct conversion of different skeletal species of the fuel components were not taken into account in the mechanism of this work.

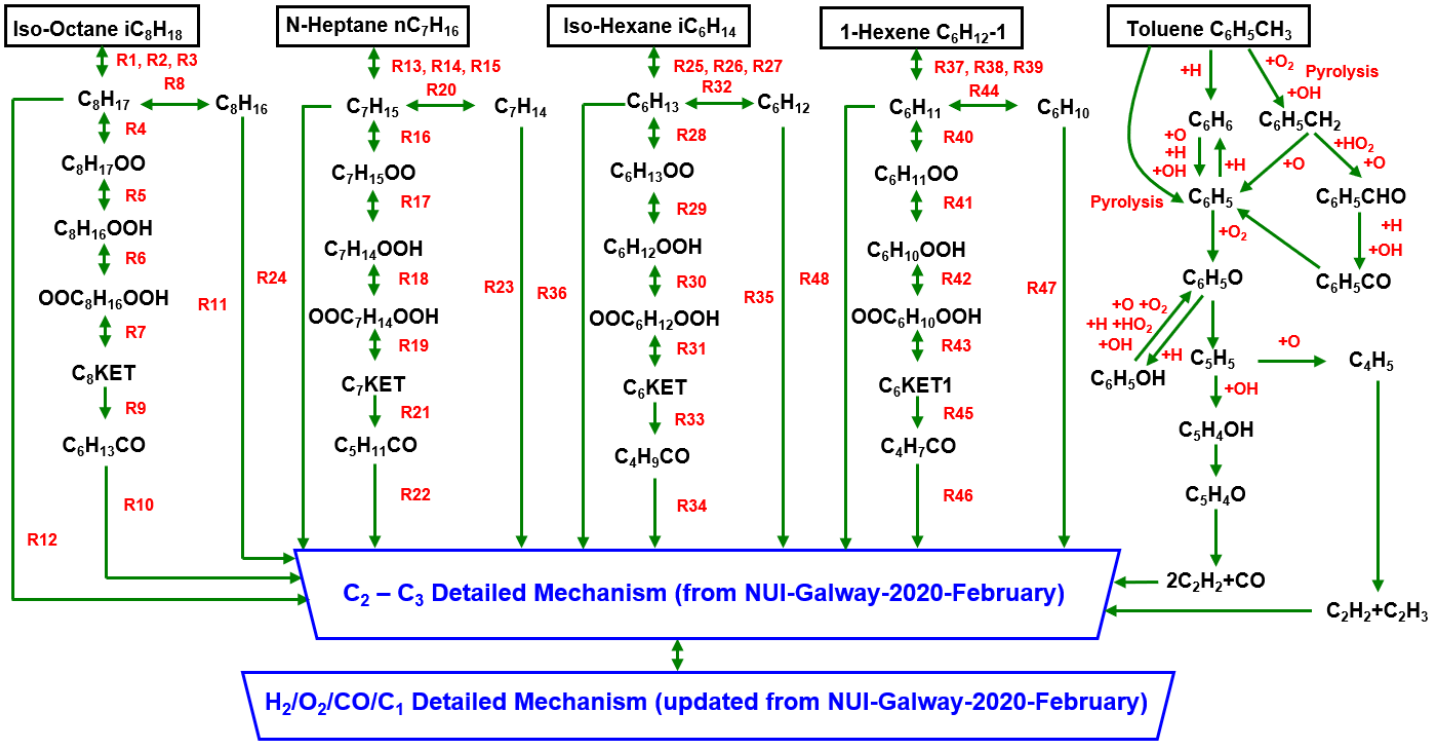

Figure 1. Overall reaction path diagram of the 5-component gasoline surrogate mechanism.

2.2 $H_2/O_2/CO$ Detailed Sub-Mechanism

The reaction $\dot{H} + O_2 \leftrightarrow \ddot{O} + \dot{O}H$ dominates the oxidation of all fuels undergoing oxidation at high temperatures (T≥1000 K). Based on two experimental datasets [31, 32], a rate constant is adopted for this

reaction over a temperature range of 1100-3370 K with a reduced uncertainty of less than 10%. A theoretical reaction rate constant calculated by Ellingson et al. [33] using *ab initio* methods based on canonical variational transition state theory with multidimensional tunneling (CVT/SCT) is used for the reaction $H_2 + H\dot{O}_2 \leftrightarrow \dot{H} + H_2O_2$ which exhibits a high sensitivity at high pressures and low temperatures found in RCM (rapid compression machine) experiments. A low-pressure limit rate constant from Bates et al. [34] over a temperature range of 1020–1260 K and over a pressure range of 10–150 bar with a high-pressure limit rate constant from Fernandes et al. [35] over a lower temperature range of 300–900 K and over a pressure range of 1.5–950 bar are combined for the chain propagation reaction $\dot{H} + O_2\,(+M) \leftrightarrow H\dot{O}_2\,(+M)$ which controls the low-temperature reactivity. A set of pressure-dependent rate constant expressions based on both experimental data and theoretical study [36] for the prediction of a wider pressure range and a wider temperature range is adopted for the reaction $H_2O_2\,(+M) \leftrightarrow \dot{O}H + \dot{O}H\,(+M)$ which is pressure-dependent. Flame speed calculations are very sensitive to the recombination reaction $\dot{H} + \dot{O}H + M \leftrightarrow H_2O + M$. Increasing the rate of this reaction decreases reactivity. Kéromnès et al. [25] have optimized the rate constant of this reaction to get the best agreement with experimental flame speed data. Flame speed predictions are also very sensitive to the reaction $H_2 + \dot{O}H \leftrightarrow \dot{H} + H_2O$ under fuel-lean conditions. A rate constant measured by Lam et al. [37] using UV (Ultraviolet) laser absorption of $\dot{O}H$ radicals behind reflected shock waves is adopted over a temperature range of 902–1518 K and a pressure range of 1.15-1.52 atm.

2.3 C_1–C_2 Detailed Sub-Mechanism

Formyl radical decomposition and hydrogen atom abstraction by molecular oxygen are primary sources of carbon monoxide in high-temperature hydrocarbon combustion. The recommendations of Friedrichs et al. [38] and Timonen et al.'s [39] measurements are used for the reaction $H\dot{C}O + M \leftrightarrow \dot{H} + CO + M$. The rate constant value for the reaction $H\dot{C}O + O_2 \leftrightarrow CO + H\dot{O}_2$ is chosen from Timonen et al. [40] who studied the reaction in a tubular reactor. The reaction $\dot{C}H_3 + \dot{O}H \leftrightarrow$ Products is very important in hydrocarbon flames. The

recommended rate constant values from Jasper et al. [41] have been refitted to a single Arrhenius expression with a minimal increase in errors. The rate constant adopted for the reaction $\dot{C}H_3 + \dot{H}(+M) \leftrightarrow CH_4(+M)$, with a high-pressure limit of $1.27\times10^{16}T^{-0.630}\exp(-193/T)$ $cm^3mol^{-1}s^{-1}$, is taken from GRI-Mech [42] as it results in the best agreement with experimental pressure-dependent methane/air laminar flame speeds. The reactions $\dot{C}H_3 + H\dot{O}_2 \leftrightarrow CH_3\dot{O} + \dot{O}H/CH_4 + O_2$ are critically important when large concentrations of methane are present. The rate constants for these reactions are taken from the theoretical work of Jasper et al. [43]. The reactions $\dot{C}H_3 + O_2 \leftrightarrow$ Products are critical in the prediction of methane ignition delays. The rate constants adopted for these reactions are from Srinivasan et al. [44] and Klippenstein [22]. The chemically activated recombination-dissociation reaction $\dot{C}H_3 + \dot{C}H_3 + M \leftrightarrow \dot{C}_2H_5 + \dot{H} + M$ has a relatively large negative sensitivity to ethane flame speeds. For this reaction, the pressure- and temperature- dependent rate expression formulated by Stewart et al. [45] has been adopted. The theoretical work of Senosiain et al. [46] has been adopted for the reaction $+ \dot{O}H \leftrightarrow$ Products, which is a very important promoting reaction in ethane oxidation. At elevated pressures, the reaction $C_2H_6 + H\dot{O}_2 \leftrightarrow \dot{C}_2H_5 + H_2O_2$ has a large influence on the reactivity of some fuels. The theoretical work of Aguilera-Iparraguirre et al. [47] has been adopted for this reaction. The formation of ethylene and a hydroperoxyl radical from the chemically activated reaction between ethyl radical and molecular oxygen $\dot{C}_2H_5 + O_2 \leftrightarrow$ Products is the most important product set at elevated temperatures. The temperature- and pressure-dependent rate recommendation from DeSain et al. [48] has been adopted for this reaction.

2.4 C_3 Detailed Sub-Mechanism

In 2020, National University of Ireland Galway developed the NUIG-Mech 1.0 mechanism [49], in which the $H_2/O_2/CO/C_1–C_3$ detailed sub-mechanisms include all the new characteristics described above, also some advancements were made on the oxidation of C_3H_6 and pyrolysis of C_2H_4. The advancements will be validated in Section 3. Beyond these new characteristics and advancements, the NUIG-Mech 1.0 mechanism especially improved the sub-mechanisms of propyne and allene for the present work in 2020. For the

improvements, new experimental data for ignition delay times (IDTs), pyrolysis speciation profiles and laminar flame speed measurements were carried out in NUIG for validating the pyrolytic and combustion characteristics of the new propyne and allene sub-mechanisms across a wide range of operating conditions. The validation [49] shows significant improvements in the predictions of IDTs, fuel pyrolysis and laminar flame speeds for propyne and allene. The improvements in fuel reactivity predictions in the new propyne and allene sub-mechanisms are due to the inclusion of the propyne + $H\dot{O}_2$ reaction class along with $\dot{O}H$ radical addition to the triple bonds on propyne and their subsequent reactions [49]. Through sensitivity and flux analyses, C_3H_4-p + $H\dot{O}_2$ and C_3H_4-p + $\dot{O}H$ addition reactions are found to be very important for propyne oxidation, particularly at low- to intermediate- temperature and high-pressure (≥ 10 bar) conditions.

2.5 Alkanes Skeletal Mechanisms

The alkanes skeletal mechanisms in this work include iso-octane, *n*-heptane, and iso-hexane mechanisms. The iso-octane and n-heptane skeletal mechanisms are taken from Liu et al. [17, 18]. Since the chemical structure of iso-hexane is similar to iso-octane, the reaction pathways of iso-hexane skeletal mechanism are similar as those of iso-octane. The reaction pathways of low temperature and decomposition in the alkanes skeletal mechanisms are based on Tananka's model [50] and Tsurushima's recommendation [51]. The H-atom abstraction from alkanes fuel, primary O_2 addition, isomerization, secondary O_2 addition to form ketohydroperoxide, and alkyl oxidation are taken from Tananka's model, as follows:

$RH+O_2=R+HO_2$ (R1, R13, R25)

$RH+OH\Rightarrow R+H_2O$ (R2, R14, R26)

$R+O_2=RO_2$ (R4, R16, R28)

$RO_2=QOOH$ (R5, R17, R29)

$QOOH+O_2=O_2QOOH$ (R6, R18, R30)

$O_2QOOH\Rightarrow C_nKET+OH$ (R7, R19, R31)

$R+O_2=olefin+HO_2$ (R8, R20, R32)

where, R represents alkyl radical or C_nH_{2n+1} structure, Q represents C_nH_{2n} structure, RO_2 represents alkylperoxy radical, QOOH represents hydroperoxyalkyl radical, O_2QOOH represents peroxyalkylhydroperoxide and C_nKET represents ketohydroperoxide. The following R3, R15, and R27 are added to maintain a balance of production and consumption of alkyl radical.

$RH+HO_2 \Rightarrow R+H_2O_2$ (R3, R15, R27)

The decomposition processes of ketohydroperoxides, R9, R21, and R33 are taken from the Tsurushima's model:

$C_nKET \Rightarrow R'CO+CH_2O+OH$ (R9, R21, R33)

where R′ represents C_6, C_5, or C_4 alkyl radicals. Considering C_3H_7, C_3H_5, C_2H_3, and C_2H_5 are primary small hydrocarbons, three simplified reactions are included in the alkanes skeletal mechanisms:

$C_6H_{13}CO+O_2 \Rightarrow C_3H_7+C_3H_5+CO+HO_2$ (R10)

$C_5H_{11}CO+O_2 \Rightarrow C_3H_7+C_2H_3+CO+HO_2$ (R22)

$C_4H_9CO+O_2 \Rightarrow C_2H_5+C_2H_3+CO+HO_2$ (R34)

The following reactions are constructed for olefin's oxidation and decomposition of alkyl radical to keep a compact size of the skeletal models as well as to fit the evolutions of n-heptane, CO, and CO_2 in JSR (jet-stirred reactor) simulation.

$C_8H_{16}+O_2 \Rightarrow C_3H_7+C_3H_6+CH_2O+HCO$ (R11)

$C_8H_{17} \Rightarrow C_3H_7+C_3H_6+C_2H_4$ (R12)

$C_7H_{14}+O_2 \Rightarrow C_3H_6+C_2H_5+CH_2O+HCO$ (R23)

$C_7H_{15} \Rightarrow C_3H_6+C_2H_5+C_2H_4$ (R24)

$C_6H_{12}+O_2 \Rightarrow C_2H_5+C_2H_4+CH_2O+HCO$ (R35)

$C_6H_{13} \Rightarrow CH_3+C_2H_4+C_3H_6$ (R36)

In the above three alkanes skeletal mechanisms, reactions (R1, R13, R25), (R6, R18, R30), and (R2, R14, R26) are key sensitive reactions for the ignition delay characteristics of iso-octane, *n*-heptane, and iso-hexane. Each alkanes (iso-octane, *n*-heptane, iso-hexane) skeletal mechanism has 8 species and 12 reactions.

2.6 Toluene Skeletal Mechanism

The toluene skeletal mechanism is mainly taken from Liu et al. [20]. The construction of the toluene skeletal mechanism is somewhat more difficult than that of alkanes skeletal mechanisms as described above due to two reasons. The first reason is that toluene is an aromatics hydrocarbon with a different molecular structure from alkanes. It is this difference that causes more complicated and diverse reaction pathways in which more species and reactions are involved. The second reason is that toluene does not have the NTC (negative temperature coefficient) effect and ignites in a relatively high temperature range (≥ 1000 K). Therefore, the high-temperature pathways for toluene oxidation have much greater influences on the ignition delay times and laminar flame speeds compared to alkanes oxidation. Considering the requirement of a compact size of the skeletal mechanism, researchers normally pay more attention to some important combustion characteristics, such as laminar flame speeds and species evolution under relatively high temperatures. To simulate the main combustion characteristics of toluene, a series of reaction paths of toluene used in different chemical kinetic mechanisms for various reactors has been adopted and an analysis of sensitivity was performed by Liu et al. [20]. Relevant reactions from the detailed mechanisms by Andrae et al. [52], Sakai et al. [53], and Mehl et al. [16] are adopted to construct the reaction paths of larger molecules in the toluene skeletal mechanism. It should be noted that the reaction '$C_6H_5CH_2+HO_2 \Rightarrow C_6H_5CHO+H+OH$' is based on the skeletal mechanism of Kim at al. [54] and Machrafi and Cavadias [55]. The toluene skeletal mechanism has 12 species and 29 reactions.

2.7 1-Hexene Skeletal Mechanism

In this work, a similar method used in the skeletal mechanisms for iso-octane, n-heptane, and iso-hexane is used to design the reaction pathways of 1-hexene skeletal mechanism. As mentioned earlier, the low-

temperature oxidation mechanism is based on Tananka's model [50] and Tsurushima's recommendation [51]. In the 1-hexene skeletal mechanism of the present work, the initial oxidation reaction at low-temperature conditions is still the H-atom abstraction reaction to form the fuel radical R. The fuel radical R reacts with O_2 via addition reaction to form alkylperoxy radical (RO_2), which can undergo isomerization reaction to form hydroperoxyalkyl radical (QOOH). QOOH can further react with O_2 through addition reaction to form peroxyalkylhydroperoxide, denoted as O_2QOOH. O_2QOOH decomposes to ketohydroperoxide (C_6KET1), which further decomposes to R′CO, CH_2O, and OH. Finally, R′CO reacts with O_2 to form small hydrocarbons. For the high-temperature oxidation mechanism of 1-hexene, the mechanism is relatively simple. The initial reactions are also mainly the H-atom abstraction reactions, then the fuel radicals decompose into smaller hydrocarbons via β-scission reactions quickly. Based on this described reaction scheme, a total number of 12 reactions constitutes the skeletal mechanism for 1-hexene, as shown below:

$C_6H_{12}\text{-}1+O_2=C_6H_{11}+HO_2$ (R37)

$C_6H_{12}\text{-}1+OH\Rightarrow C_6H_{11}+H_2O$ (R38)

$C_6H_{12}\text{-}1+HO_2\Rightarrow C_6H_{11}+H_2O_2$ (R39)

$C_6H_{11}+O_2=C_6H_{11}O_2$ (R40)

$C_6H_{11}O_2=C_6H_{10}OOH$ (R41)

$C_6H_{10}OOH+O_2=O_2C_6H_{10}OOH$ (R42)

$O_2C_6H_{10}OOH\Rightarrow C_6KET1+OH$ (R43)

$C_6H_{11}+O_2=C_6H_{10}+HO_2$ (R44)

$C_6KET1\Rightarrow C_4H_7CO+CH_2O+OH$ (R45)

$C_4H_7CO+O_2\Rightarrow C_2H_3+C_2H_3+CO+HO_2$ (R46)

$C_6H_{10}+O_2\Rightarrow C_2H_3+C_2H_4+CH_2O+HCO$ (R47)

$C_6H_{11}\Rightarrow C_3H_5+C_3H_6$ (R48)

In this 1-hexene skeletal mechanism, reactions (R37), (R38), and (R40) are key sensitive reactions for the ignition delay characteristics of 1-hexene. 1-hexene skeletal mechanism has 8 species and 12 reactions.

2.8 Optimization of Reaction Rate Constants of Skeletal Mechanisms

Cai and Pitsch [56, 57] developed an optimization method and its extension for optimizing a reduced mechanism based on general reaction rate rule for various hydrocarbon fuels. In their method the rates for reaction classes are calibrated instead of the modification of rates of single elementary reactions leading to a chemically more consistent model optimization. In the present work, the reaction rate constants of the recently advanced $H_2/O_2/CO/C_1$ and $C_2–C_3$ detailed sub-mechanisms keep unchanged since they are widely and well validated. Since laminar flame speeds are mainly controlled by the $H_2/O_2/CO/C_1$ and $C_2–C_3$ detailed sub-mechanisms, the reaction rate constants are not needed to be optimized for the performance of laminar flame speeds. However, ignition delay times and major species mole fractions are mainly controlled by skeletal mechanisms (from raw fuel to C_4 species), thus the optimization of reaction rate constants will only focus on the pre-exponential factors of some reactions of the five skeletal mechanisms. If Cai and Pitsch's method is used in this work, some well-determined reaction rate constants in the $H_2/O_2/CO/C_1$ and $C_2–C_3$ detailed sub-mechanisms may be changed. Therefore, instead of using Cai and Pitsch's optimization method, a method similar to Chang et al.'s work [21] as well as Ra and Reitz's work [58] was used to optimize the reaction rate constants of skeletal mechanisms of iso-octane, n-heptane, iso-hexane, 1-hexene and toluene individually.

There are six steps for ignition delay optimization. In step 1, four characteristic points are chosen on the ignition delay curve, which are a low temperature point (less than the start of NTC regime), NTC crest, NTC valley, and a high temperature point (greater than the end of NTC regime). According to the order of the difference between experiment and simulation for the four picked points, the four points are renamed as Point 1, Point 2, Point 3, and Point 4. In step 2, ignition delay sensitivity analysis for the four points is performed, also the sensitive reactions of each point are ranked. In step 3, at Point 1 which has the largest difference between

experimental and simulated ignition delay times, the pre-exponential factor A of the reaction which has the largest absolute sensitivity coefficient value at Point 1 is optimized to achieve a good match between experiment and simulation. In step 4, the ignition delay at Point 2 is initially checked. If the ignition delay is not good, the pre-exponential factor A of the reaction which has the largest absolute sensitivity coefficient value at Point 2 but is not included in the sensitive reactions of Point 1 is optimized. In step 5, the ignition delay at Point 3 is initially checked. If the ignition delay is not good, the pre-exponential factor A of the reaction which has the largest absolute sensitivity coefficient value at Point 3 but should not be included in the sensitive reactions of Points 1 & 2 or has the least impacts on Points 1 & 2 is optimized. In step 6, the optimization of Point 4 is similar to step 5. There are three steps for JSR major species mole fractions optimization. In step 1, four characteristic temperature points are chosen on the mole fraction curve. In step 2, sensitivity analysis of absolute rate of production (ROP) and sensitivity analysis of consumption of fuel are conducted to find out the sensitive reactions of each characteristic point. In step 3, similar steps used in the above ignition delay optimization process can be used for JSR major species mole fractions optimization. After the JSR major species mole fractions optimization is finished, an iterative optimization of both ignition delay and JSR major species mole fractions is needed, until the optimized reactions can satisfy both ignition delay times and major species mole fractions.

Brute-force sensitivity analysis is used in the above optimization process. Equation (1) is the definition of sensitivity of ignition delay time:

$$\text{Sensitivity}=\frac{\tau_{ign}(2k_i)-\tau_{ign}(k_i)}{\tau_{ign}(k_i)} \tag{1}$$

In equation (1), k_i is the rate constant of reaction i, $\tau_{ign}(2k_i)$ is the ignition delay time when the rate constant of reaction i has been doubled, and $\tau_{ign}(k_i)$ is the nominal value of the ignition delay time. Thus, a positive value of sensitivity means that the ignition delay becomes longer when the rate constant of reaction i is doubled,

hence the reactivity is decreased, and vice-versa. The definition of sensitivity of major species mole fractions is similar to equation (1).

3. RESULTS AND DISCUSSIONS

The proposed 5-component gasoline surrogate chemical kinetic mechanism has been validated using various reactant mixtures to investigate the effectiveness of each sub-mechanism: $H_2/O_2/CO$ detailed sub-mechanism, C_1-C_2 detailed sub-mechanism, C_3 detailed sub-mechanism, iso-octane skeletal mechanism, n-heptane skeletal mechanism, toluene skeletal mechanism, iso-hexane skeletal mechanism, and 1-hexene skeletal mechanism. The same entire mechanism was used in the simulations for validating each sub-mechanism. To validate each sub-mechanism, various experimental data from the literature were used, including ignition delay times from either shock tube or rapid compression machine, laminar flame speeds, major species concentration profiles in either jet-stirred reactor or flow reactor. The CHEMKIN model setup for ignition delay includes: problem type: constrain pressure and solve energy equation (default); absolute tolerance: 1.0E–20; relative tolerance: 1.0E–8; sensitivity absolute tolerance: 1.0E–6; sensitivity relative tolerance: 0.0001; maximum number of iterations: 4; select temperature inflection point; ignition temperature delta: 400.0K. For laminar flame speed the CHEMKIN model setup includes: maximum number of grid points allowed: 250; number of adaptive grid points: 10; adaptive grid control based on solution gradient: 0.8 (continuation#1: 0.4, continuation#2: 0.1); adaptive grid control based on solution curvature: 0.8 (continuation#1: 0.4, continuation#2: 0.1); starting axial position: 0.0 cm; ending axial position: 10.0 cm; absolute tolerance: 1.0E–9; relative tolerance: 0.0001; absolute tolerance for pseudo time stepping: 1.0E–9; relative tolerance for pseudo time stepping: 0.0001; number of time steps: 100.0; windward differencing. For JSR the CHEMKIN model setup includes: problem type: fix gas temperature; steady state solver; absolute tolerance: 1.0E–9; relative tolerance: 0.0001; absolute tolerance for pseudo time stepping: 1.0E-9; relative tolerance for pseudo time stepping: 0.0001; number of time steps: 100.0. Only a part of the validation results about the recently advanced

$H_2/O_2/CO/C_1–C_3$ detailed sub-mechanisms is presented in this paper to show the performances of the new characteristics and advancements/improvements compared to existing chemical kinetic models.

3.1 Validation Results of the $H_2/O_2/CO$, $C_1–C_2$, and C_3 Detailed Sub-Mechanisms

The simulation from the present mechanism has been performed and compared to the experimental data under stoichiometric conditions with 100%, 50%, 25%, and 10% H_2 in H_2/CO fuel mixtures with nitrogen dilution at an end-of-compression pressure of 70 bar and an end-of-compression temperature range of 914–1068 K. The experimental data in Figure 2 show the inhibiting effect of carbon monoxide on the syngas ignition delay times, which increase with increasing amounts of CO in the syngas mixture. The model captures this inhibiting effect accurately and its predictions are in very good agreement with the experimental results. The simulated laminar flame speeds from the present mechanism have been compared to the experimental data for an H_2/CO fuel mixture with helium dilution at an initial temperature of 298 K, an equivalence ratio range of 0.5–3.5, and various initial pressures. As shown in Figure 3, the present model (Sim_new) shows a good prediction compared to the experimental data, also the inhibiting effect of pressure on the syngas laminar flame speeds can be well captured by the present model. The results from the $H_2/O_2/CO$ sub-mechanism used in Liu et al. [17, 18, 20] are also shown in Figure 3 for comparison (represented by Sim_old). Overall, the present mechanism is closer to the experimental data than the old mechanism.

The measured species profiles presented in the work of Kéromnès et al. [25] as functions of time for $H_2/O_2/N_2$ mixture in a flow reactor over broad pressure and temperature ranges (0.5~14 atm and 750~1100 K respectively) were used in the present work. The simulations from the present mechanism have been carried out and compared to the measured species data. As shown in Figure 4, the present mechanism can well reproduce the measured species data and the temperature dependence of hydrogen consumption. It must be pointed out that for the flow reactor simulation it is necessary to shift the time in order to match the point at which 50% of the fuel is consumed. This practice is commonly used by some researchers (e.g. Kéromnès et al. [25]) in order

to take into account any reactivity occurring during the initial mixing of reactants, where non-ideal conditions are encountered.

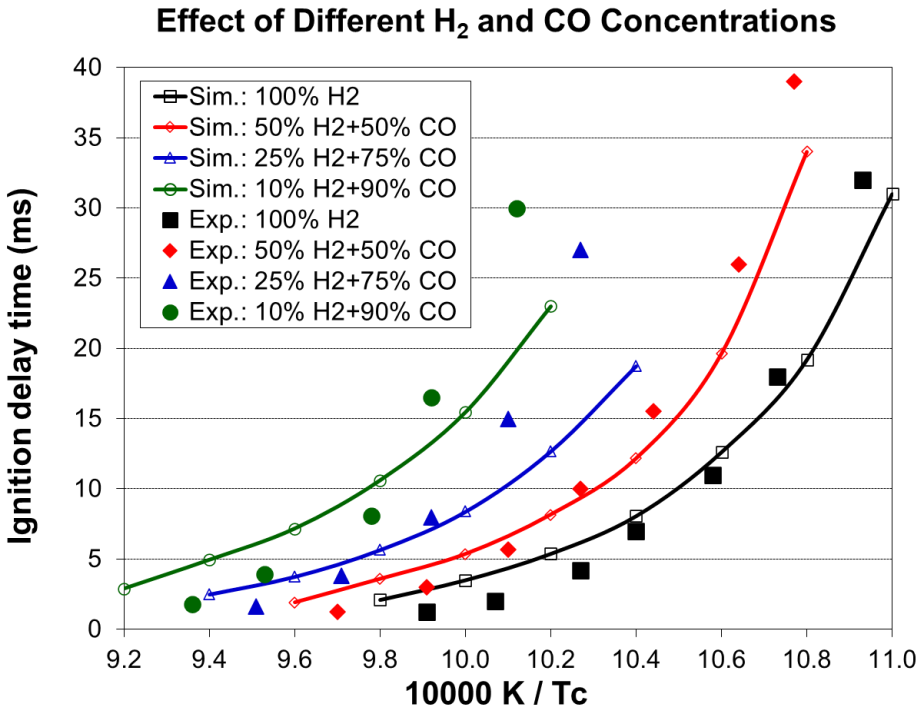

Figure 2. Effect of different H_2 and CO concentrations on ignition delay times (Pc=70 bar, 12.5% (αH_2+(1-α)CO)+6.25% O_2+81.25% N_2, experimental data are taken from [25])

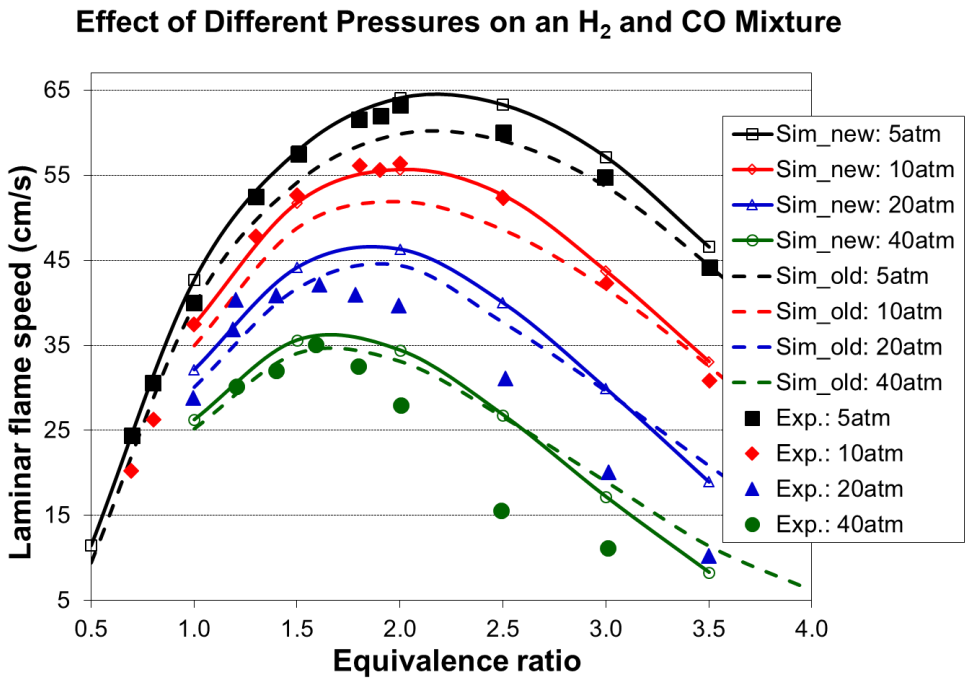

Figure 3. Comparisons between measured flame speeds and calculated flame speeds from this work (95% CO + 5% H_2 in O_2 + 7 He, Ti = 298 K, experimental data are taken from [25])

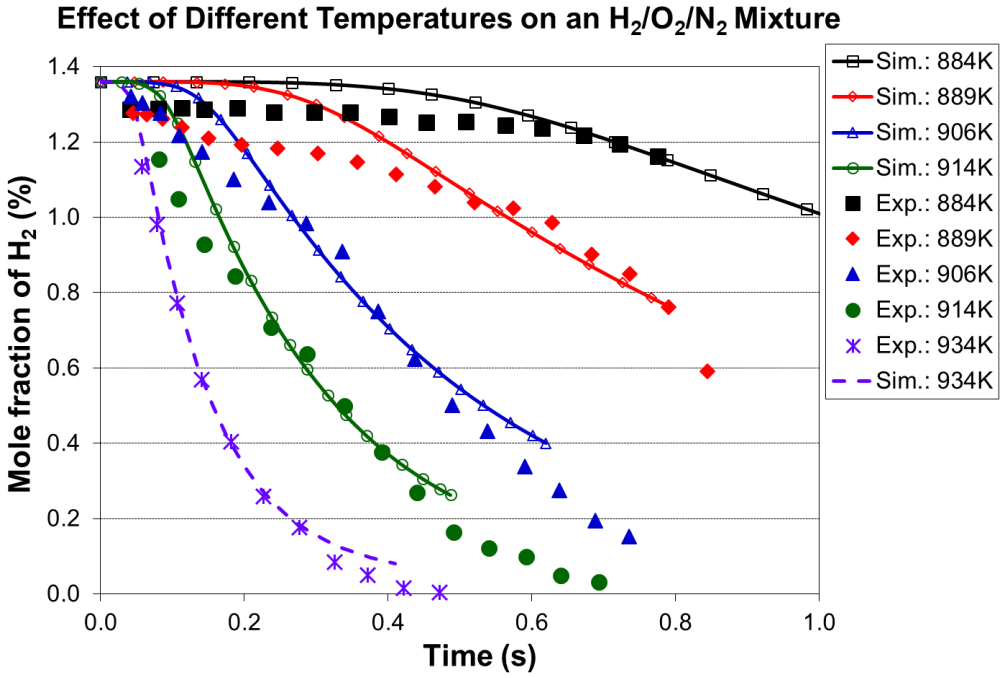

Figure 4. Comparisons between measured and calculated H_2 profiles in a flow reactor under various initial temperatures at 6.5 atm ($H_2/O_2/N_2$=1.36/2.24/96.4, experimental data are taken from [25])

The effect of different dilution ratios ($D=O_2/(O_2+N_2)$) on the laminar flame speeds of a mixture of propene, O_2, and N_2 at p = 1 atm and T = 298 K was simulated and compared to experimental data. The dilution levels were: 0.18, 0.19, 0.20, 0.209 (air). Even a minor modification of the dilution ratio will lead to significant change in the laminar flame speed as shown in Figure 5(a), and this effect can be well captured by the present mechanism. Using the old mechanism of Liu et al. [17, 18, 20], the effect of different dilution levels on the laminar flame speeds of the same mixture of Figure 5(a) under the same condition is shown in Figure 5(b). Compared to the results shown in Figure 5(a) from using the present new mechanism, the prediction shown in Figure 5(b) from using the old mechanism is much higher than the experimental data for equivalence ratio greater than 0.9. The reason may be that the C_2–C_3 sub-mechanism of the old model is just a simply reduced sub-mechanism. Figure 6 shows the simulation of concentration profiles of some species in a jet-stirred reactor with a C_3H_6/O_2/He mixture and comparison with the experimental data. The equivalence ratio is 2.19, the temperature ranges 800–1100 K, and the pressure is near atmospheric. Overall, the present mechanism can accurately predict the oxidation of propene in a JSR under fuel-rich conditions, predicting the consumptions of fuel and oxygen as well as the formations of major intermediate and product species correctly.

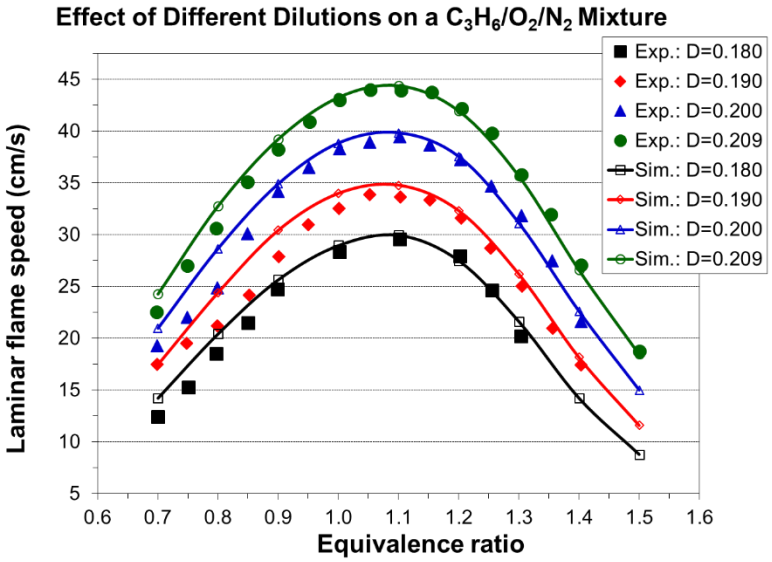

(a) Results from the present new C_2–C_3 and $H_2/O_2/CO/C_1$ detailed sub-mechanisms

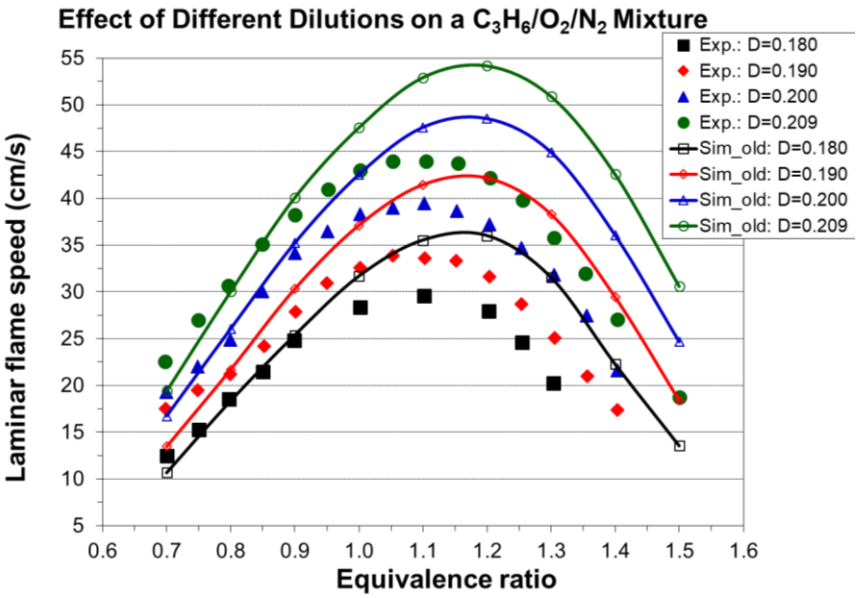

(b) Results from the old C_2–C_3 and $H_2/O_2/CO/C_1$ mechanisms of Liu et al. [17, 18, 20]

Figure 5. Effect of different dilution levels on the laminar flame speeds of a propene, O_2, and N_2 mixture at p = 1 atm and T = 298 K (dilution level D=$O_2/(O_2+N_2)$, experimental data are taken from [29])

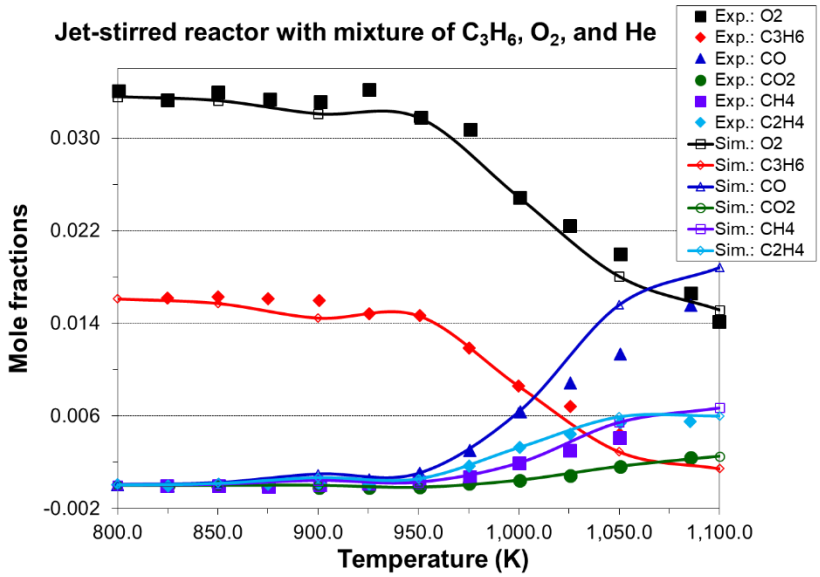

Figure 6. Simulated species mole fractions in a jet-stirred reactor with a mixture of 1.64% propene, 3.38% O_2 in He, φ = 2.19, p = 1.05 atm, residence time=2.0 s, and compared to jet-stirred reactor experimental data (experimental data are taken from [28])

C_3H_6 is a key species in the recently advanced $H_2/O_2/CO/C_1$-C_3 detailed sub-mechanisms. Figure 7 shows the ignition delay times of a stoichiometric C_3H_6/air mixture versus temperature under various initial pressures from the advanced $H_2/O_2/CO/C_1$–C_3 detailed sub-mechanisms, the existing Aramco 3.0 mechanism [59] which is widely used currently by many researchers, as well as the experimental data provided by NUI-Galway. From Figure 7, it is seen that the new model not only predicts the ignition delay times of the propene/air mixture under various pressures very well but also is much better than the Aramco 3.0 mechanism, also there is no ignition from the Aramco 3.0 mechanism at the pressure of 30 bar.

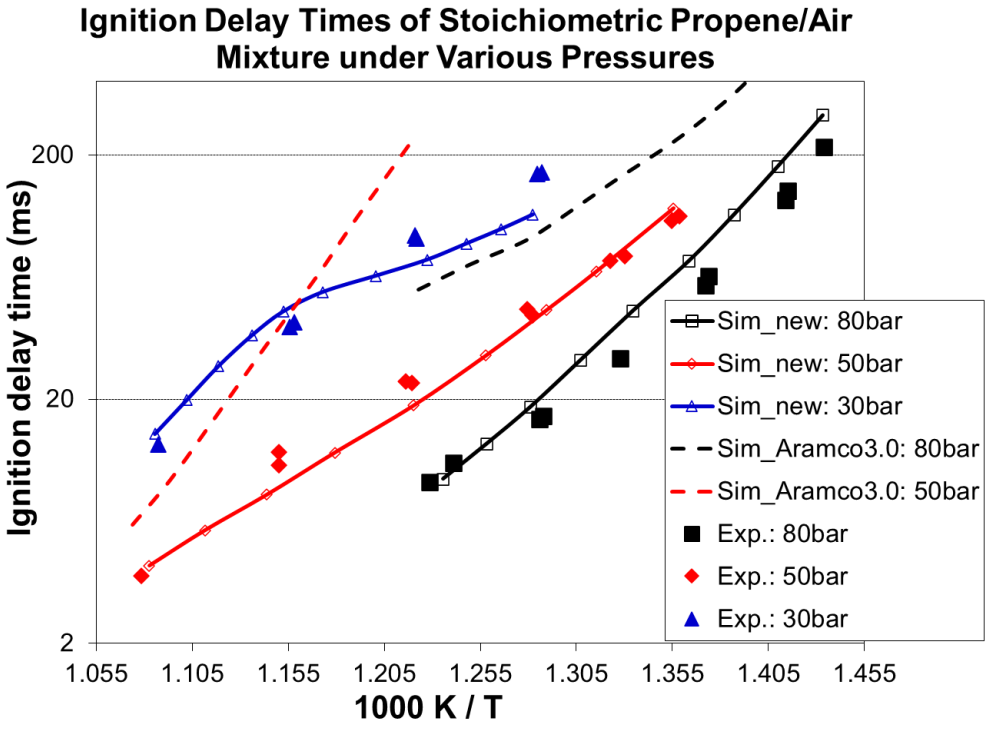

Figure 7. Ignition delay times of a stoichiometric C_3H_6/air mixture under various pressures (experimental data were provided by National University of Ireland Galway).

C_2H_4 is another key species in the recently advanced $H_2/O_2/CO/C_1$–C_3 detailed sub-mechanisms. Figure 8 shows the mole fractions of ethylene and acetylene versus temperature during the pyrolysis of 1% of C_2H_4 in a shock tube at a pressure of 1 atm from the advanced $H_2/O_2/CO/C_1$–C_3 detailed sub-mechanisms, the existing AramcoMech3.0 mechanism, as well as experimental shock tube data provided by NUI-Galway. From

Figure 8, it is seen that compared to the experimental data the present advanced $H_2/O_2/CO/C_1–C_3$ detailed sub-mechanisms have a much better performance than the existing AramcoMech3.0 mechanism in terms of the prediction of mole fractions of ethylene and acetylene during the pyrolysis of ethylene.

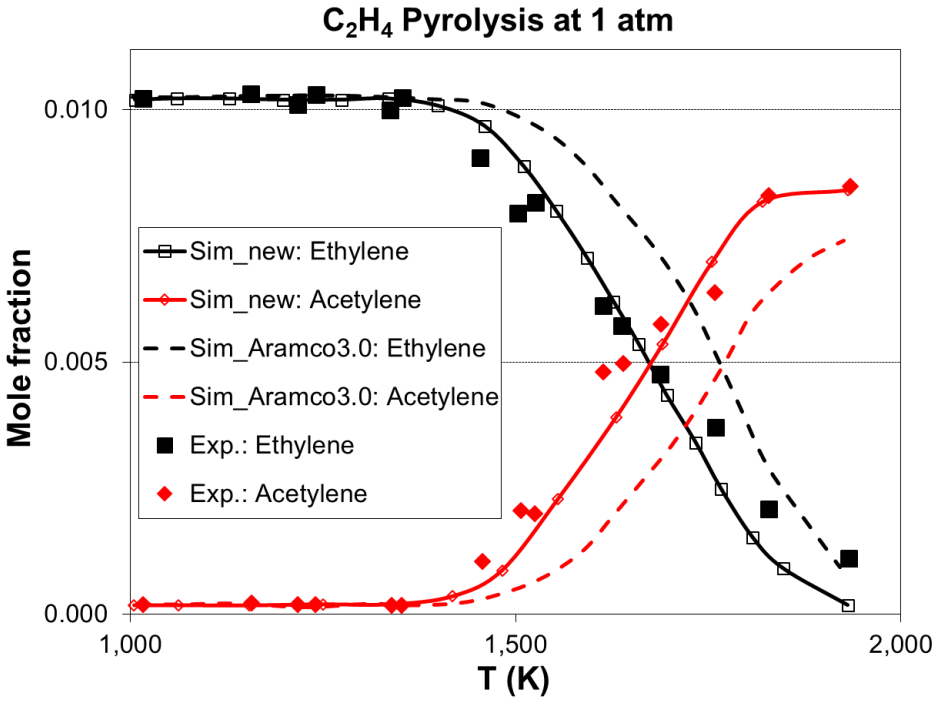

Figure 8. Mole fractions of ethylene and acetylene during the pyrolysis of 1% of C_2H_4 at 1 atm (experimental shock tube data were provided by National University of Ireland Galway).

Figure 9 shows the ignition delay time measurements provided by NUI-Galway and modeling results from the new mechanism of this work for propyne/'air' (O_2 and N_2/Ar) [49] mixtures at pressures of 30 atm and 10 atm for (a) and (b), respectively. The low and high temperature data are from rapid compression machine and high-pressure shock tube experiments, respectively. The experimental data also include RDC (reaction during compression) periods. The criteria for ignition delay time is based on maximum rate of pressure rise. For comparison, the modeling results from the existing Aramco 3.0 mechanism are also shown in Figure 9.

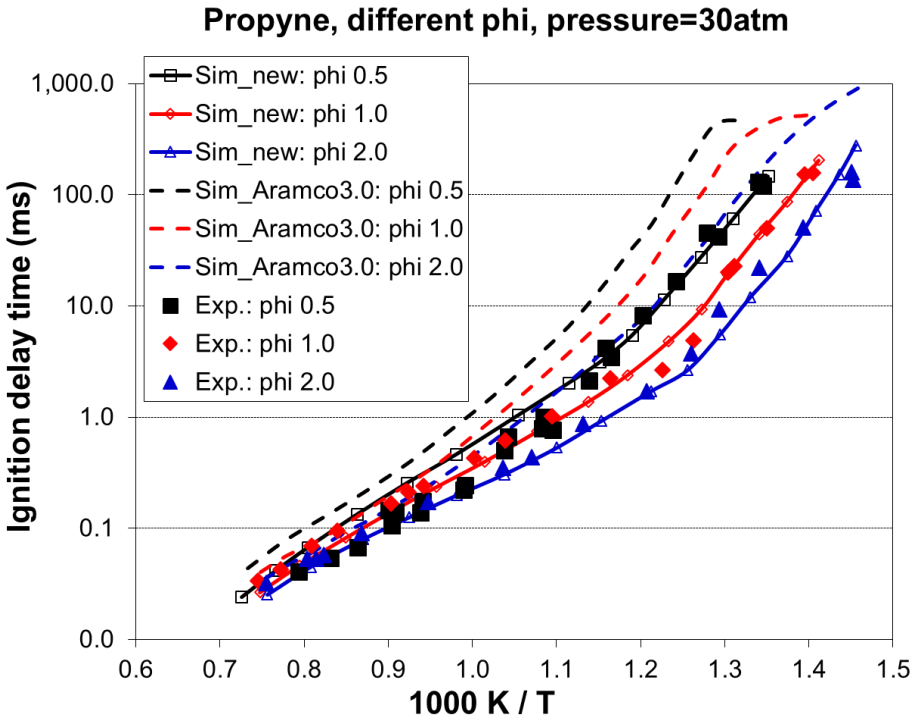

(a) $p = 30$ atm.

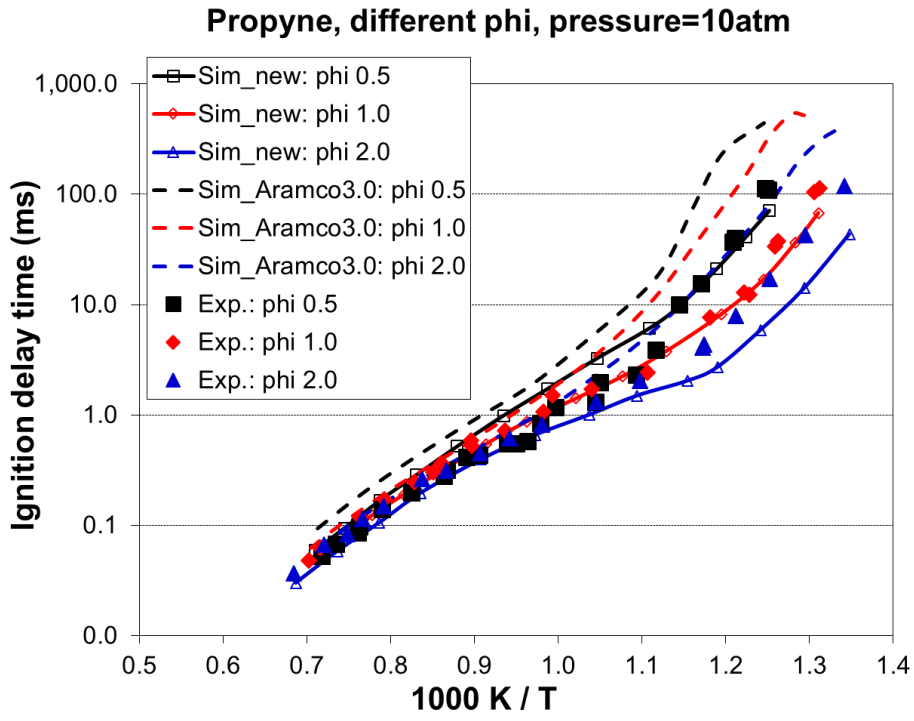

(b) $p = 10$ atm.

Figure 9. Ignition delay time measurements and modeling results for propyne in 'air' mixtures.

Figure 9 shows a significantly improved performance of the new propyne sub-mechanism contained in the present advanced $H_2/O_2/CO/C_1–C_3$ detailed sub-mechanisms, particularly at low temperatures (< 1000 K). It can also be seen that ignition delay times decrease with increasing temperature and equivalence ratio, as expected. However, the effect of equivalence ratio on the ignition delay time declines at high temperatures. The present new propyne sub-mechanism captures all of the experimental data trends very well but tends to under-predict the reactivity at $\varphi = 2.0$ and at $p = 10$ atm for the lower-temperature RCM experiments. Compared to the existing Aramco 3.0 mechanism, the present advanced $H_2/O_2/CO/C_1–C_3$ detailed sub-mechanisms offer better agreements.

3.2 Validation Results of Iso-Octane Skeletal Mechanism

The ignition delay time comparison between the simulation using the present mechanism and the shock tube experimental data from Fieweger et al. [60] for iso-octane/air mixtures is shown in Figure 10. Both the simulated main and first stage ignition delay times show very good agreements with the experimental data except at the temperature range of 800~870 K for the equivalence ratio of 2.0. The NTC behavior for the two equivalence ratios (1.0 and 2.0) and the influence of equivalence ratio on ignition delay time are reproduced quite well. Since the advanced $H_2/O_2/CO/C_1$-C_3 detailed sub-mechanisms are used, the reaction rate constants of the iso-octane skeletal mechanism have to be re-optimized. The method described in Section 2.8 was used for the re-optimization. Figure 11 shows the laminar flame speed comparisons between simulation and experimental data for iso-octane/air mixtures at various initial temperatures. It can be seen that the present mechanism performs quite well against the experimental data from lean mixtures to rich mixtures. Figure 12 shows the comparisons of iso-octane, CO and CO_2 concentrations in a jet stirred reactor between simulation and experimental data for an iso-octane/O_2/N_2 stoichiometric mixture. The experimental profiles of fuel, CO and CO_2 are well reproduced using the present mechanism, although the predicted profile of CO_2 has a slight shift

toward lower temperatures and the simulated profile of CO is slightly under-estimated in the temperature range of 950~1100 K.

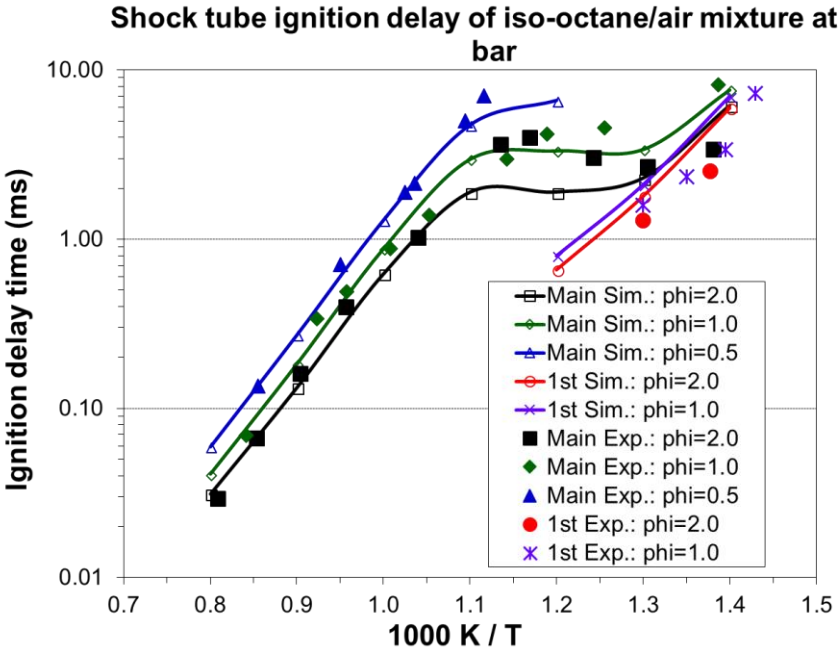

Figure 10. Ignition delay comparison between simulation and experiment [60] for iso-octane/air mixtures.

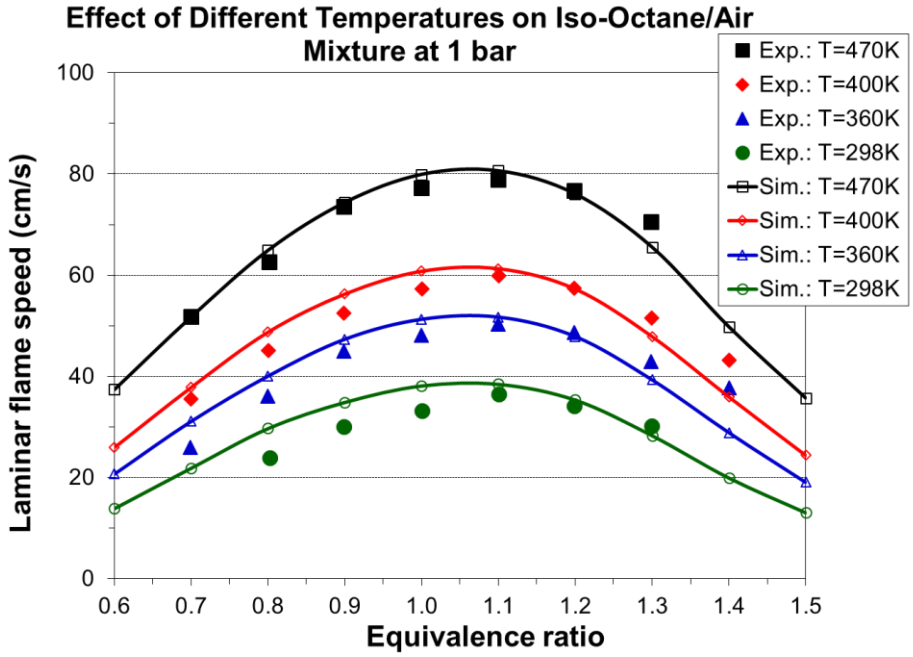

Figure 11. Laminar flame speed comparisons between simulation and experiment [61] for iso-octane/air mixtures at an initial pressure of 1 bar and various initial temperatures.

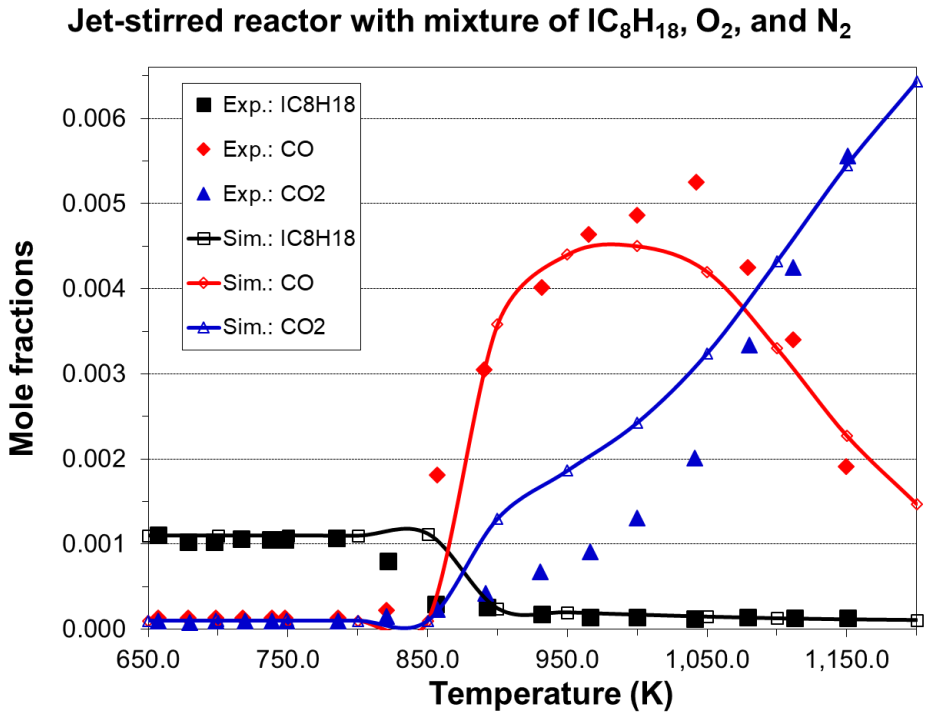

Figure 12. Comparisons of some species concentrations in a jet stirred reactor between simulation and experiment [62] for an iso-octane/O_2/N_2 stoichiometric mixture at an initial pressure of 10 bar (residence time = 1.0 s, 0.1% iso-octane).

3.3 Validation Results of N-Heptane Skeletal Mechanism

The ignition delay time comparison between the simulation using the present mechanism and the shock tube experimental data from Ciezki et al. [63] for an *n*-heptane/air mixture is shown in Figure 13. It can be seen that the simulated main ignition delay times show very good agreements with the experimental data at various pressures for stoichiometric equivalence ratio. The NTC behavior of each of the four pressures (1.35, 1.93, 3.0, 4.2 MPa) and the influence of pressure on ignition delay time are reproduced quite well using the present mechanism. The reaction rate constants of the present n-heptane skeletal mechanism were updated using the optimization method described in Section 2.8. Figure 14 shows the ignition delay time comparisons between the simulation and the experimental data from Fieweger et al. [60] for various PRF blends. It can be seen that the influence of octane number on ignition delay time is also reproduced quite well using the present mechanism.

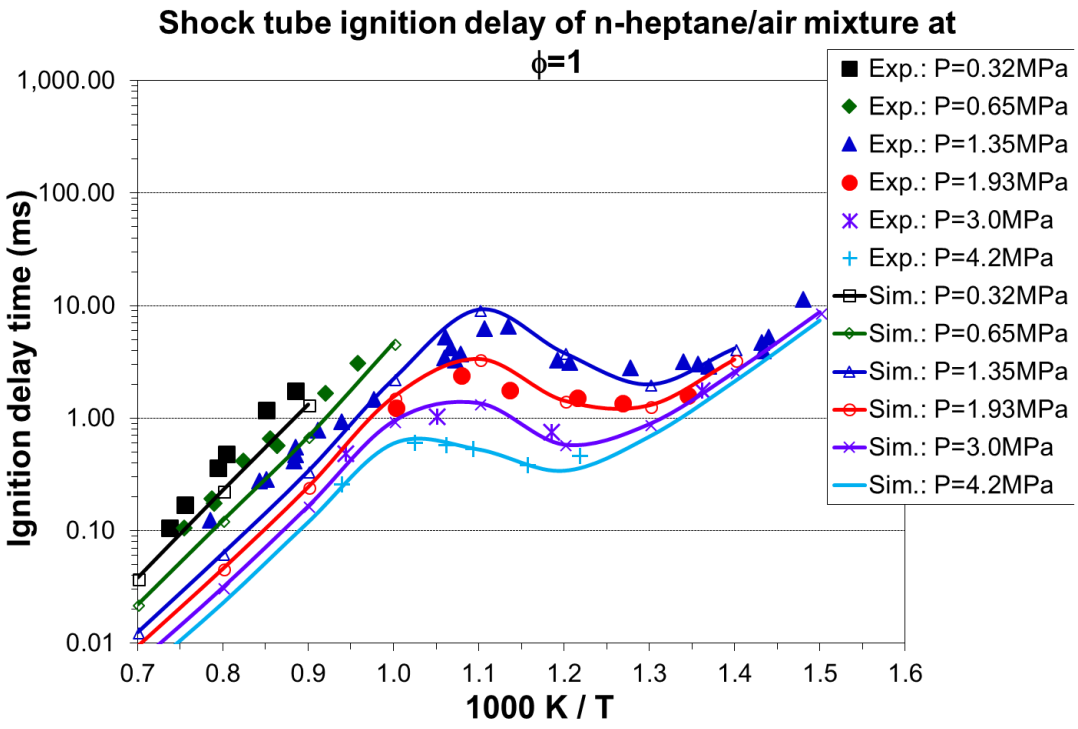

Figure 13. Ignition delay comparison between simulation and experiment [63] for an n-heptane/air mixture

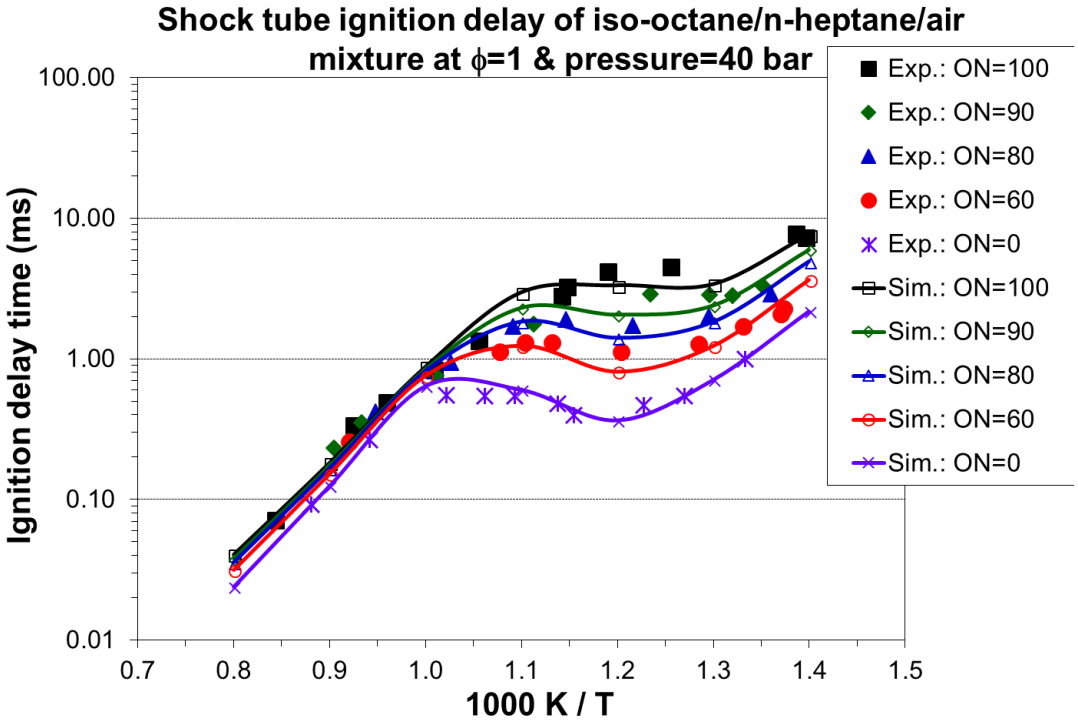

Figure 14. Ignition delay comparisons between simulation and experiment [60] for various PRF blends.

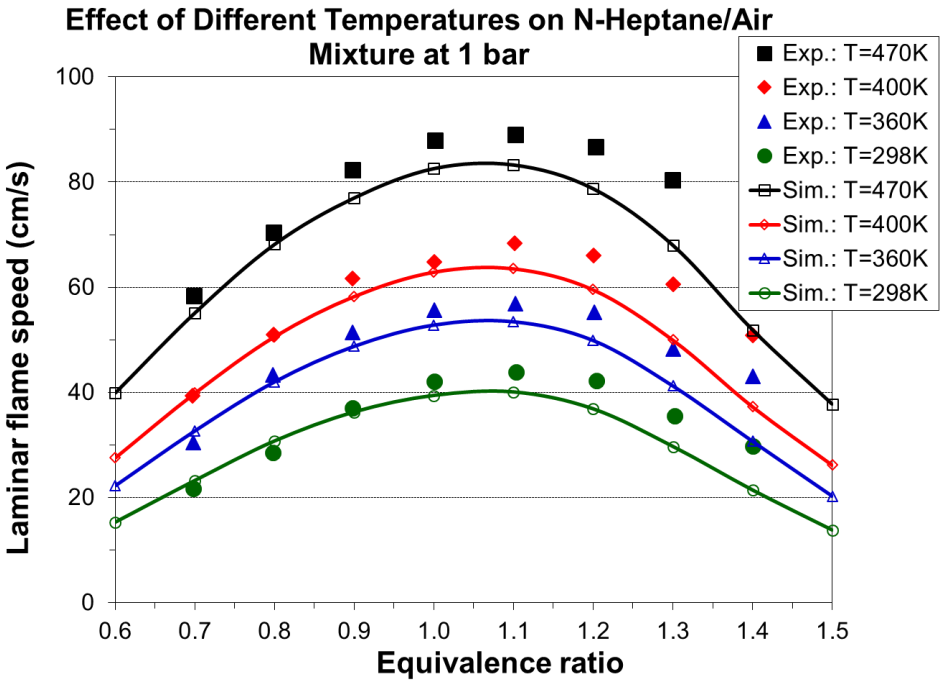

Figure 15. Laminar flame speed comparisons between simulation and experiment [61] for n-heptane/air mixtures at an initial pressure of 1 bar and various initial temperatures.

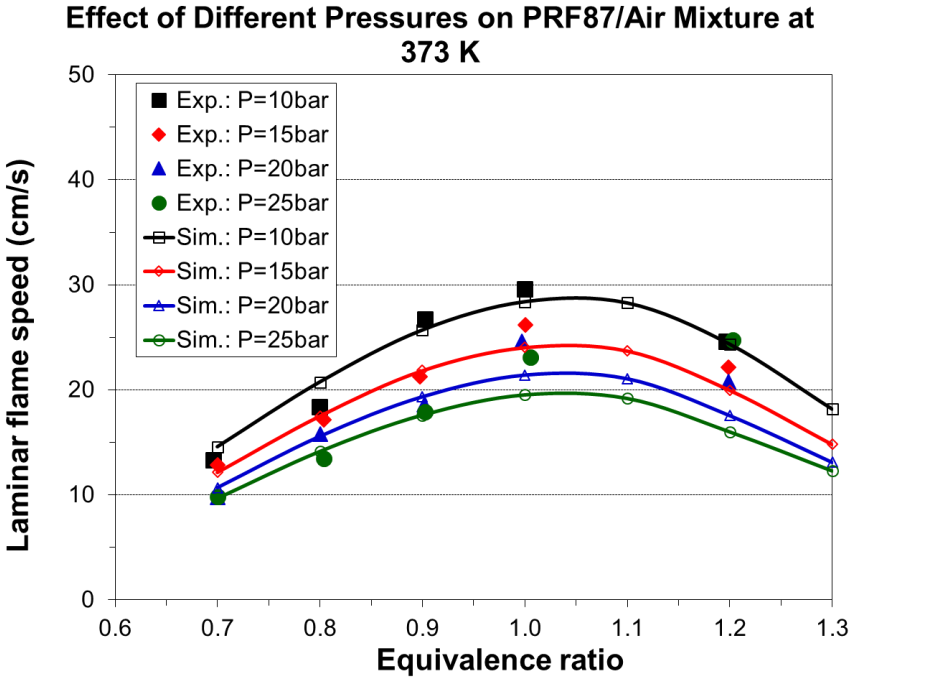

Figure 16. Laminar flame speed comparisons between simulation and experiment [64] for PRF87/air mixtures at an initial temperature of 373 K and various initial pressures.

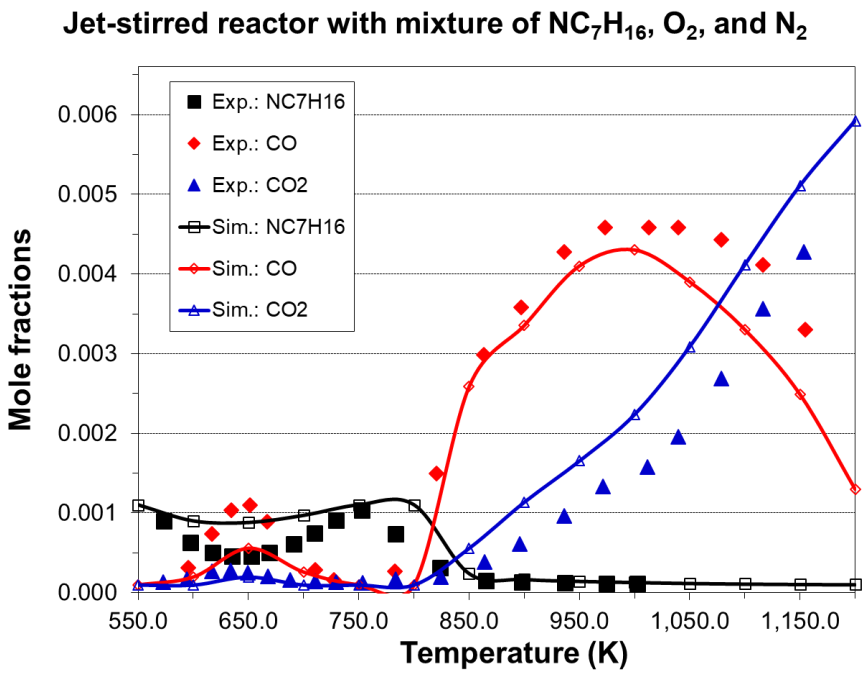

Figure 17. Comparisons of species concentrations between simulation and experiment [62] for an *n*-heptane/O_2/N_2 stoichiometric mixture at an initial pressure of 10 bar (residence time = 1.0 s, 0.1% *n*-heptane).

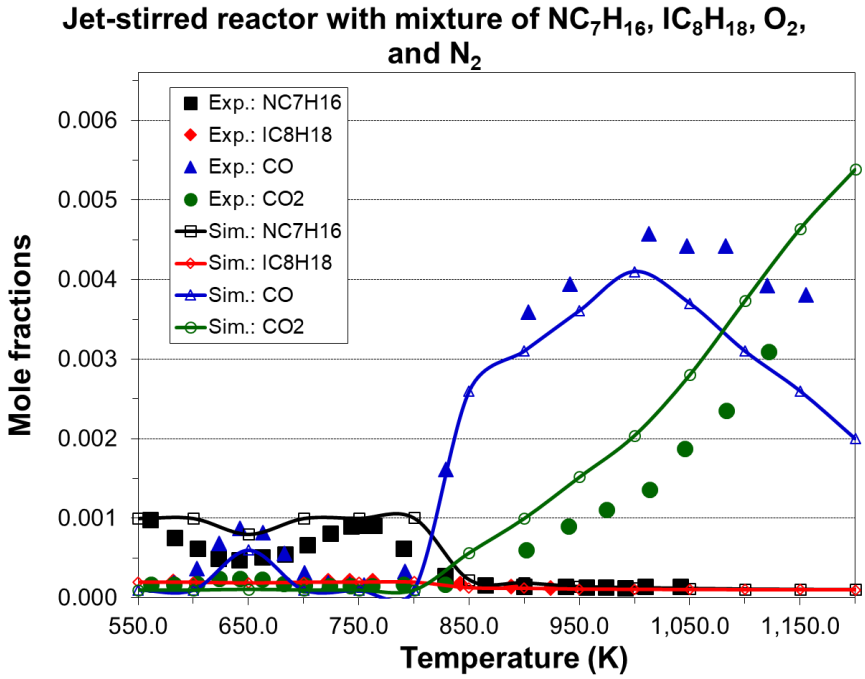

Figure 18. Comparisons of species concentrations in a jet stirred reactor between simulation and experiment [65] for a PRF10/O_2/N_2 stoichiometric mixture at an initial pressure of 10 bar (residence time=1.0 s, 0.1% fuel).

Figure 15 shows the laminar flame speed comparisons between the simulation using the present mechanism and the experimental data for n-heptane/air mixtures at various initial temperatures. It can be seen that the present mechanism performs well against the experimental data from lean to stoichiometric mixtures although the simulation is a little lower than the experiment for rich mixtures. Figure 16 shows the laminar flame speed comparisons between simulation and the experimental data from Jerzembeck et al. [64] for PRF87/air mixtures at an initial temperature of 373 K and various initial pressures. The present mechanism performs well against the experimental data for 10 bar and 15 bar from lean to rich mixtures. For 20 bar and 25 bar, although the present mechanism provides satisfactory simulations of laminar flame speeds for lean mixtures, it produces lower values for rich mixtures than the experimental data. Since the experimental data in Figure 16 were obtained for gasoline (octane number = 87), the same case will be revisited in Section 3.7 using the 5-component gasoline surrogate model of this work. The comparisons of n-heptane, CO and CO_2 concentrations between simulation and experiment for a stoichiometric n-heptane/O_2/N_2 mixture in a jet-stirred reactor are shown in Figure 17. For a stoichiometric PRF10/O_2/N_2 mixture in a jet-stirred reactor, the comparisons of fuel (iso-octane and n-heptane), CO and CO_2 concentrations between simulation and experiment are shown in Figure 18. From Figures 17 and 18, it can be seen that the experimental profiles of fuel (n-heptane, iso-octane), CO and CO_2 can be well reproduced using the present mechanism below 950 K. However, the CO concentration is underpredicted at temperatures above 950 K, while the CO_2 concentration is overpredicted at temperatures above 950 K, indicating that a higher conversion rate of CO to CO_2 is produced by the present mechanism. The reason may be mainly due to the omitted reaction pathways of large molecules' decomposition.

3.4 Validation Results of Toluene Skeletal Mechanism

The ignition delay time comparison between the simulation using the present mechanism and the shock tube experimental data from Shen et al. [66] for a toluene/air stoichiometric mixture at a pressure of 5.0 MPa is shown in Figure 19. Overall, the ignition delay time simulated by the present mechanism shows a good

agreement with the experimental data under the pressure and stoichiometric equivalence ratio. The reaction rate constants of the present toluene skeletal mechanism have been re-optimized using the optimization method described in Section 2.8.

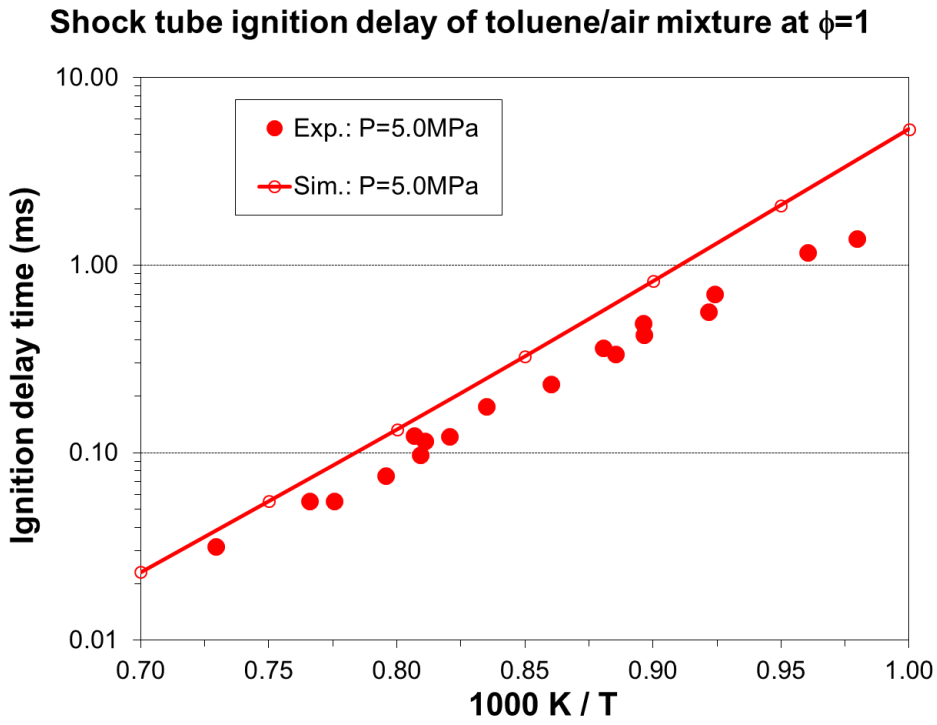

Figure 19. Ignition delay comparison between simulation and experiment [66] for a toluene/air mixture.

The ignition delay time comparisons between the simulation and the experimental data from Hartmann et al. [67] are shown in Figures 20 (a) and (b) for an n-heptane/toluene/air mixture and an iso-octane/toluene/air mixture, respectively. It can be seen that the NTC behavior for the n-heptane/toluene/air mixture can be well captured and the simulated ignition delay times show very good agreements with the experimental data for both n-heptane/toluene/air and iso-octane/toluene/air mixtures. Figure 21 shows the laminar flame speed comparisons between the simulation and the experimental data for toluene/air mixtures at various initial temperatures/pressures. It can be seen that the predicted laminar flame speeds for all equivalence ratios under 1 bar/298 K and lean mixtures under 3 bar/450 K are lower than the experimental data, although the present mechanism performs well against the experimental data from stoichiometric to rich mixtures under 3 bar/450 K.

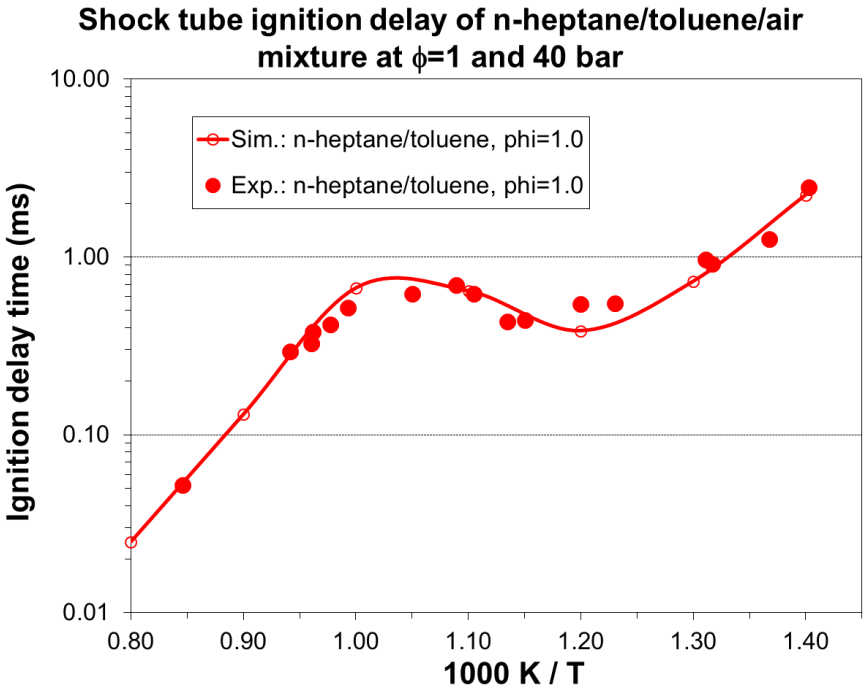

(a)

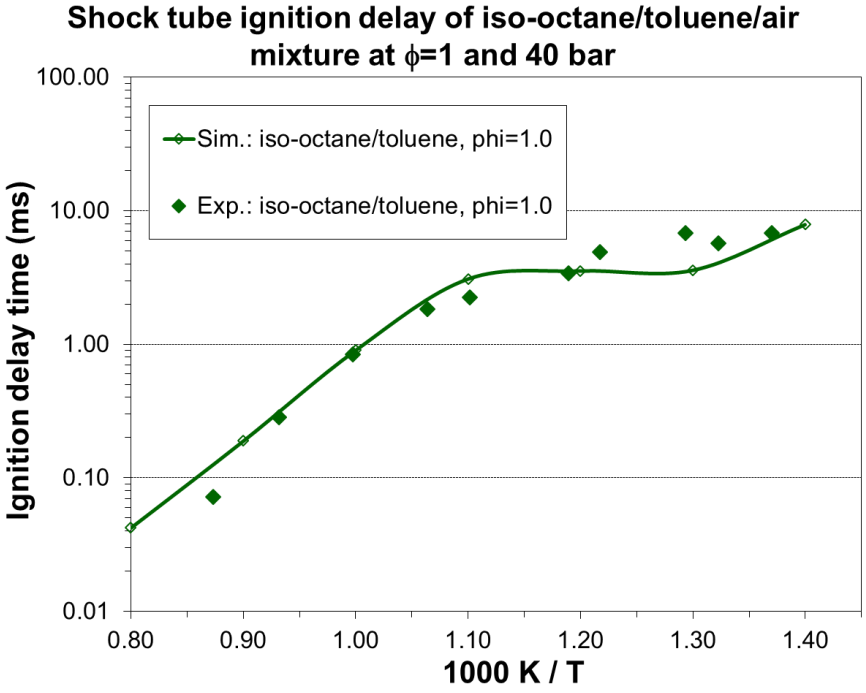

(b)

Figure 20. Ignition delay comparison between simulation and experiment [67] in a shock tube for an n-heptane/toluene/air (a) or an iso-octane/toluene/air (b) stoichiometric mixture at p = 4.0 MPa.

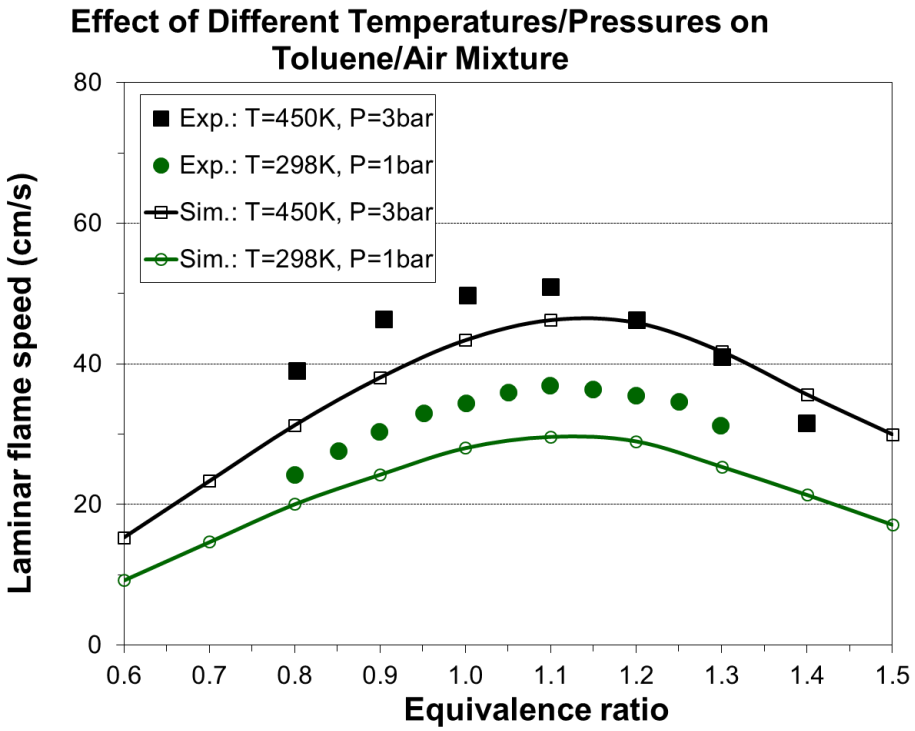

Figure 21. Laminar flame speed comparisons between simulation and experiment [69, 70] for toluene/air mixtures at various initial temperatures/pressures.

One possible reason for the discrepancy shown in Figure 21 is that some reaction paths and species which are eliminated in the toluene skeletal mechanism might have certain influences on the prediction of laminar flame speeds. However, the good thing is that the experimental data under quite low pressures are not representative for engine-relevant conditions. Figure 22 shows the laminar flame speed comparisons between the simulation and the experimental data from Zhao et al. [68] for mixtures of unleaded conventional gasoline (CR-87, octane number = 87) and air at an initial pressure of 1 bar and two initial temperatures of 353 K and 500 K. The results show that the predictions using the present mechanism match the experimental data well for the two initial temperatures. In the simulation a gasoline surrogate as used in Liu et al. [20] (RON = 88.0, MON = 85.0, H/C = 1.971, Iso-octane mole fraction = 56%, Toluene mole fraction = 28%, *n*-heptane mole fraction = 17%) was used in Figure 22. The comparisons of some important species (toluene, CO and CO_2) concentrations between simulation and experiment for a stoichiometric toluene/O_2/N_2 mixture with highly diluted nitrogen in a

jet-stirred reactor are shown in Figure 23. From Figure 23, it can be seen that the profiles of toluene, CO and CO_2 simulated using the present mechanism match the experimental data well. However, the peak value of CO at around 1000 K is underpredicted. Figure 24 shows the comparisons of ignition delay times between experiment and simulation using the same surrogate as in Figure 22 without EGR (exhaust gas recirculation) in a pressure range of 45~60 bar. The results show that the ignition delay times computed by the present mechanism match the experimental data well, except for stoichiometric and rich mixtures at temperatures lower than 833 K. It should be pointed out that the experimental data in Figures 22 and 24 were obtained for gasoline/air mixtures whereas the simulation results were obtained from a three-component (iso-octane, n-heptane, toluene) gasoline surrogate which may not correctly represent the physical/chemical properties of the gasoline fuel used in the experiments. The cases in Figures 22 and 24 will be revisited in Section 3.7 using the 5-component gasoline surrogate model of this work.

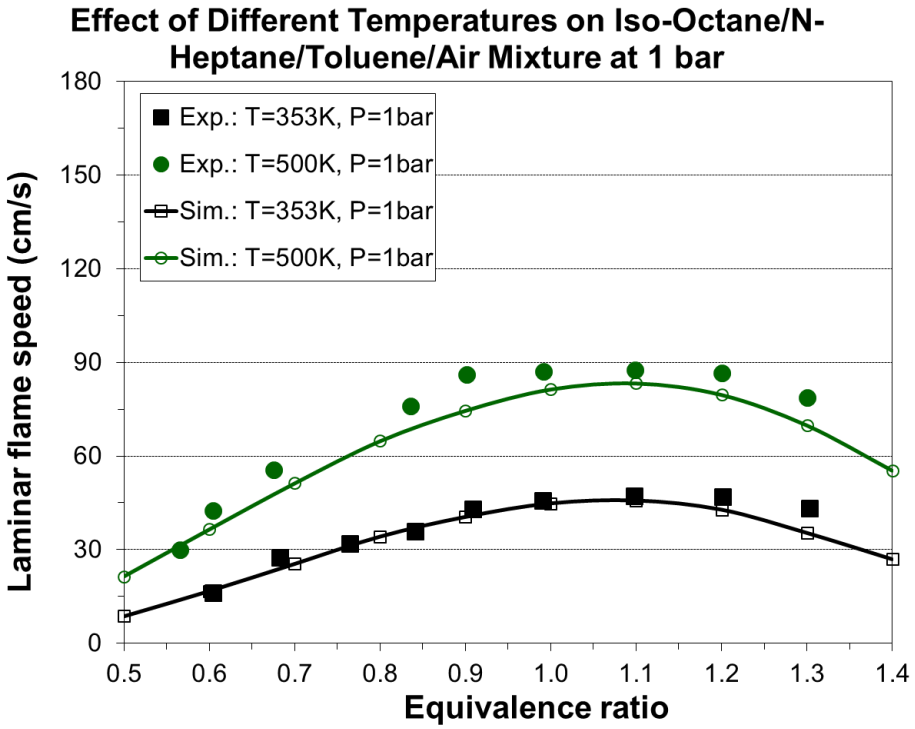

Figure 22. Laminar flame speed comparisons between simulation and experiment [68] for gasoline/air mixtures at an initial pressure of 1 bar and various initial temperatures.

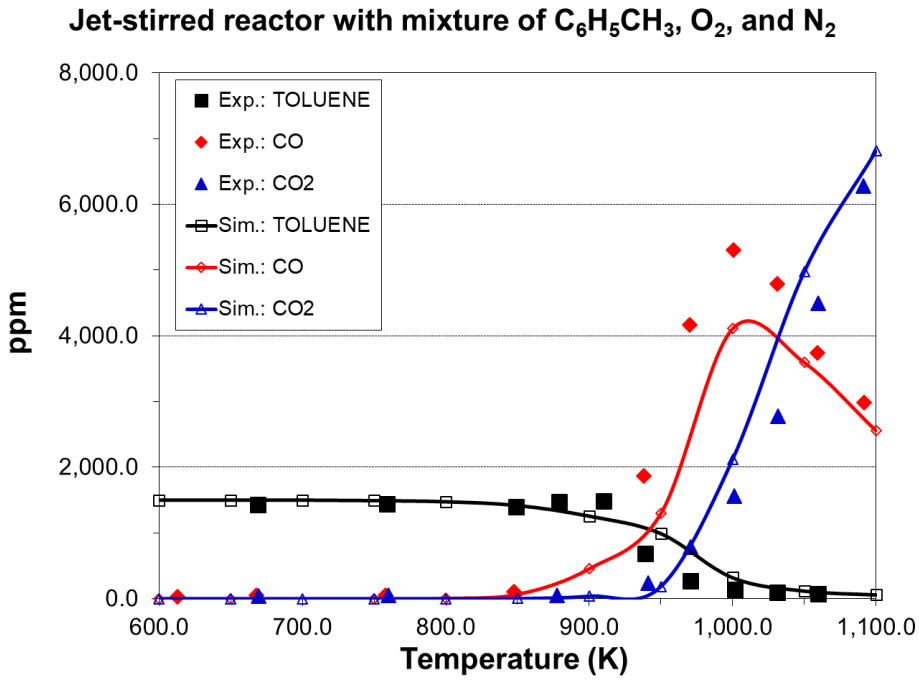

Figure 23. Comparisons of species concentrations between simulation and experiment [71] for a toluene/O_2/N_2 mixture at an initial pressure of 10 bar (φ = 1.0, residence time = 1.0 s, 0.15% toluene, 1.35% O_2).

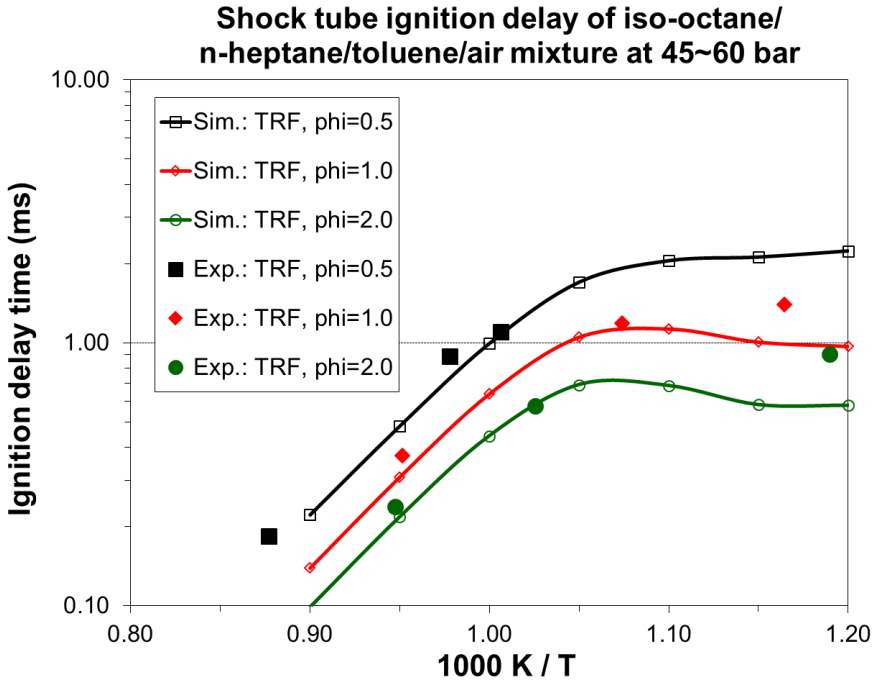

Figure 24. Shock tube ignition delay comparisons between simulation and experiment [72] for gasoline/air mixtures at various pressures, temperatures, and equivalence ratios.

3.5 Validation Results of 1-Hexene Skeletal Mechanism

The ignition delay time comparison between the simulation using the present mechanism and the shock tube or rapid compression machine experimental data from Yang et al. [73] for 1-hexene/air mixtures is shown in Figure 25. It can be seen that the simulated ignition delay times show very good agreements with the experimental data from lean to rich mixtures under pressures of 1.2~15 bar and temperatures of 600~1600 K. To the best of the authors' knowledge, fewer experimental studies have been performed to obtain ignition delay times at other conditions for 1-hexene. The reaction rate constants of the present 1-hexene skeletal mechanism are obtained using the optimization method described in Section 2.8. Fan et al. [74] performed experimental measurements of laminar flame speeds of 1-hexene/air mixtures at various initial pressures. Figure 26 shows the laminar flame speed comparisons between the simulation using the present mechanism and the experimental data for 1-hexane/air mixtures at an initial temperature of 373 K and various initial pressures. As the pressure increases, the laminar flame speed decreases with a nonlinear behavior. The trend of this decrease is well captured by the present mechanism. Also, the present mechanism performs well against the experimental data from ϕ=0.7 to ϕ=1.5 for different pressures. Figure 27 shows the comparisons of 1-hexene, O_2, CO and CO_2 concentrations in a jet stirred reactor between the simulation using the present mechanism and the experimental data from Meng et al. [75] for 1-hexene/O_2/He mixtures at atmospheric pressure with different equivalence ratios and temperatures between 500 K and 1100 K. It can be seen that the experimental profiles of fuel, O_2, CO and CO_2 are well reproduced using the present mechanism for lean and stoichiometric mixtures. Overpredictions of the fuel and O_2 consumptions and an underprediction of the CO formation are observed at high-temperature conditions for rich mixtures. As demonstrated by the experimental designers [75], there may

be large errors of experimental measurements at these conditions due to saturation of the cavity-ring down spectroscopy (CRDS) experimental signals, which makes the experimental measurements less accurate [75].

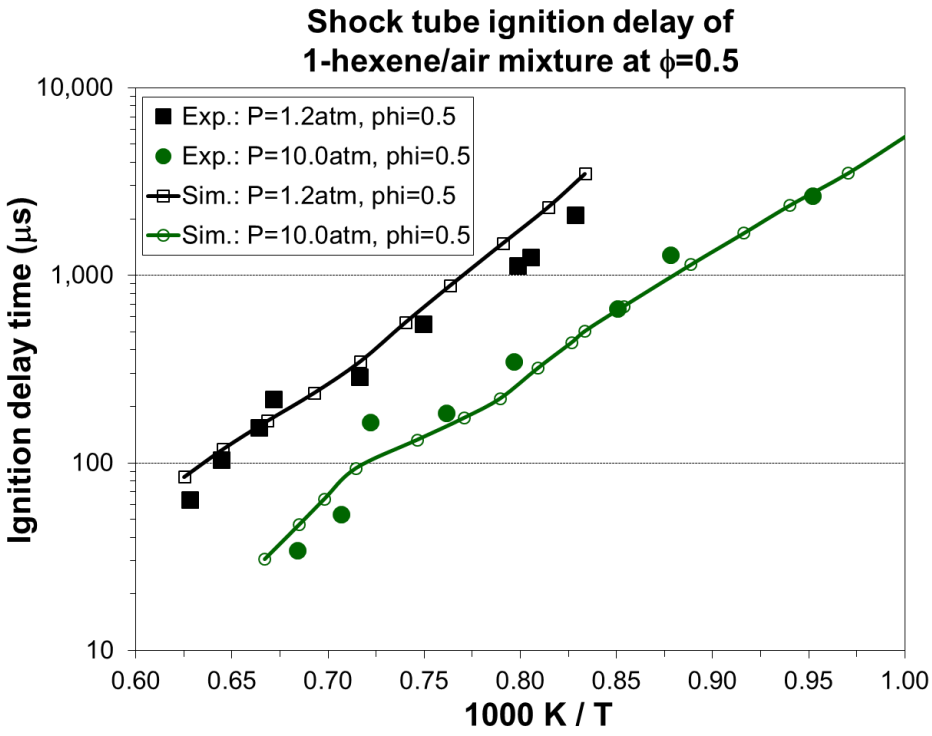

(a) phi = 0.5.

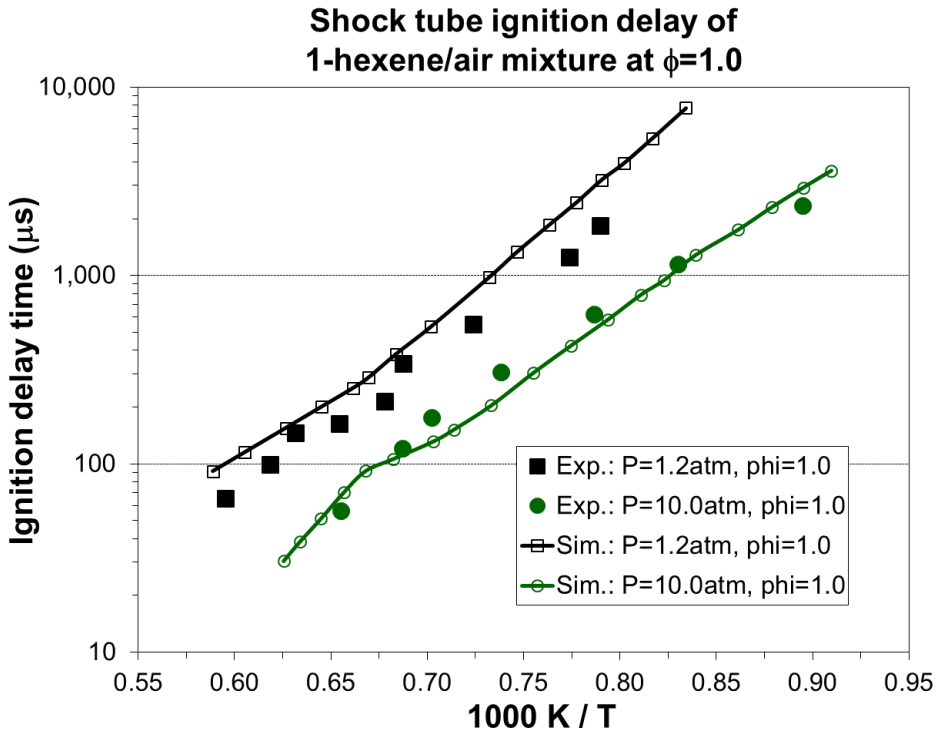

(b) phi = 1.0.

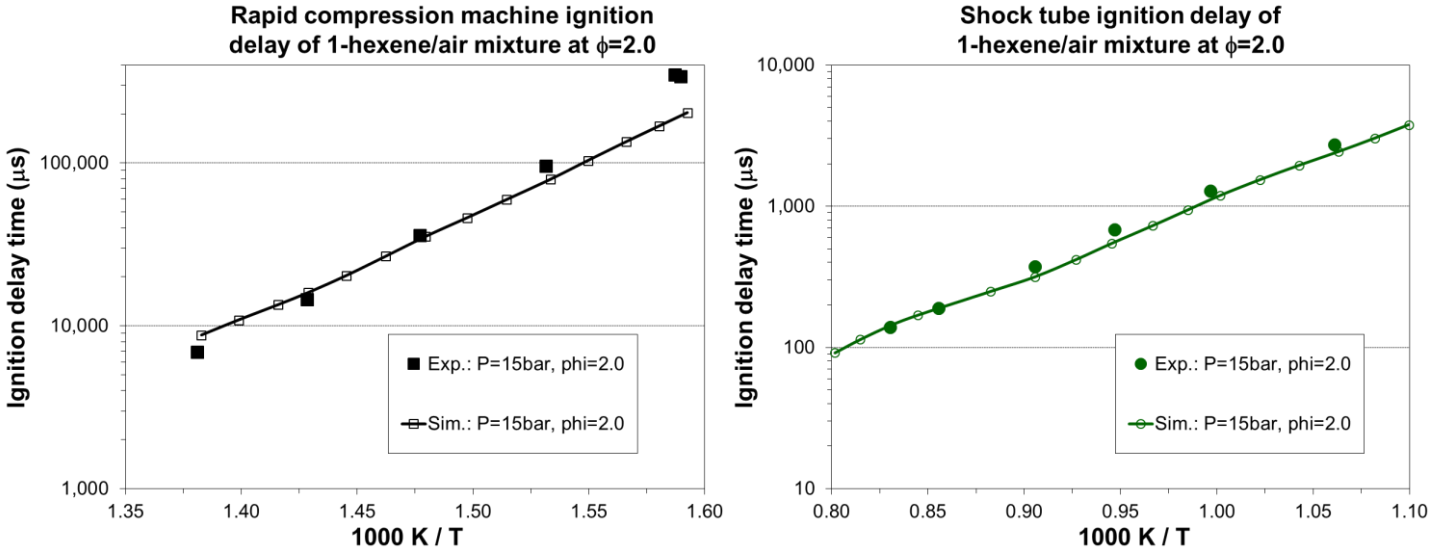

(c) phi = 2.0

Figure 25. Ignition delay comparison between simulation and experiment [73] for 1-hexene/air mixtures.

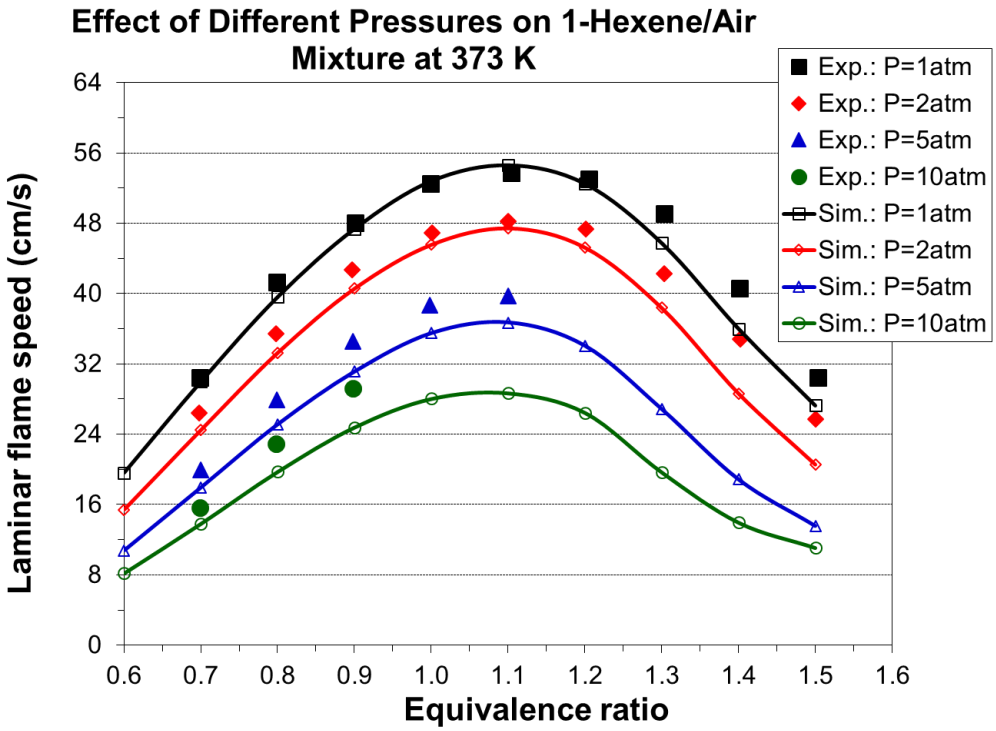

Figure 26. Laminar flame speed comparisons between simulation and experiment for 1-hexene/air mixtures at an initial temperature of 373 K and various initial pressures (experimental data are taken from [74]).

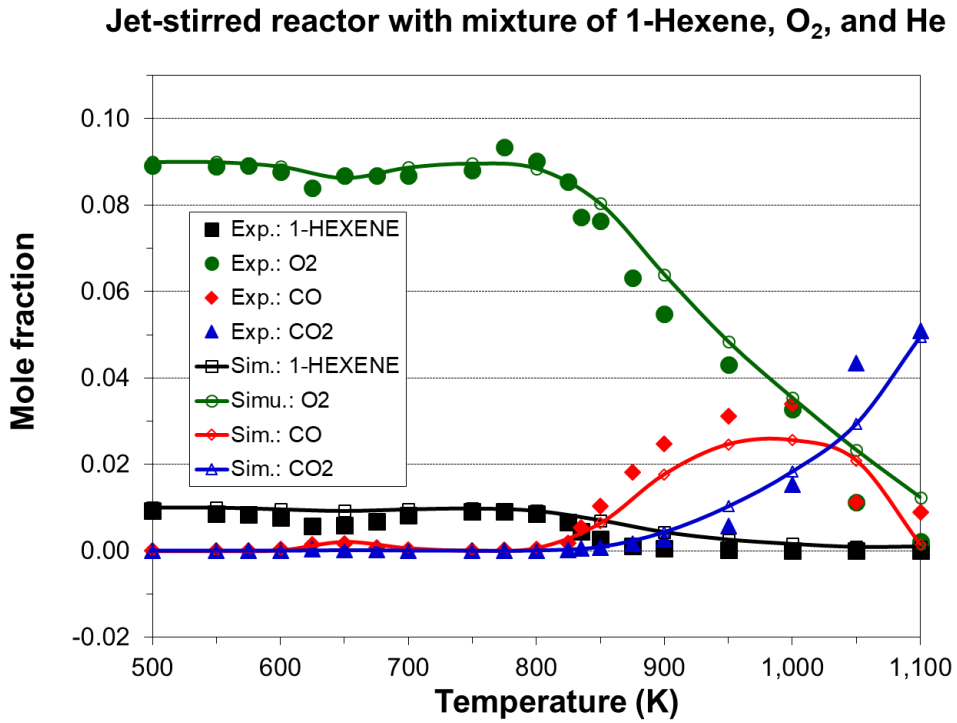

(a) phi = 1.0.

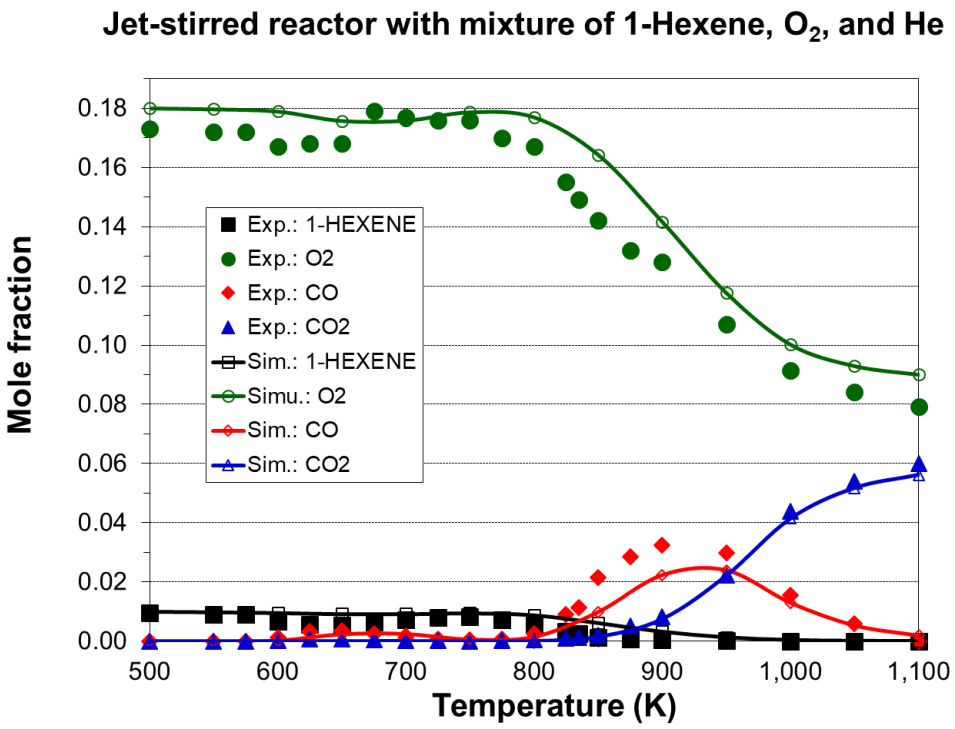

(b) phi=0.5

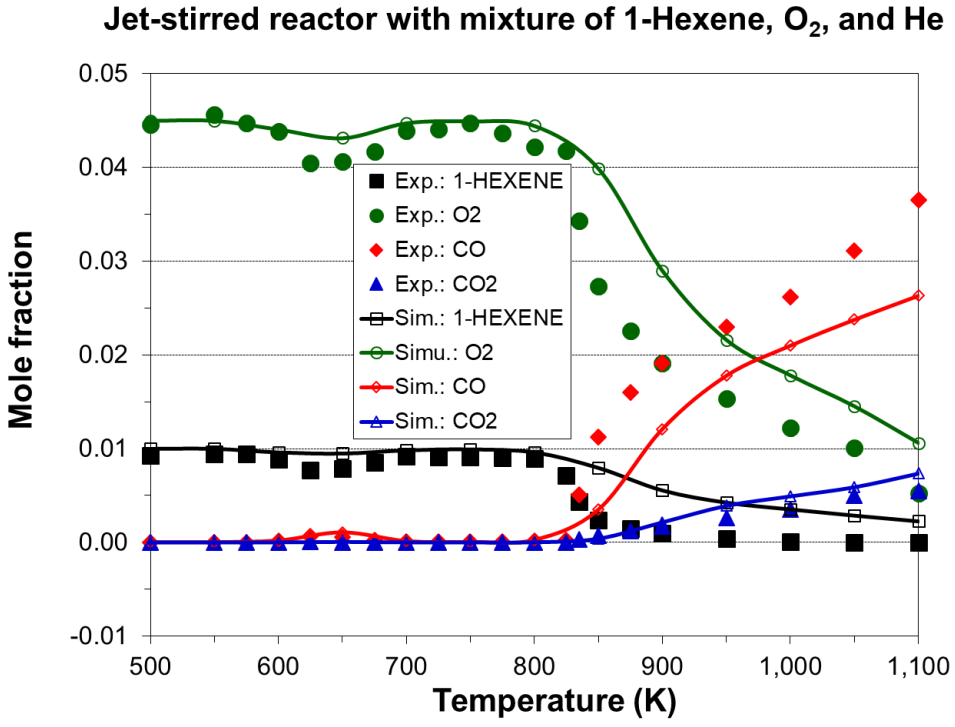

(c) phi = 2.0.

Figure 27. Comparisons of some species concentrations in a jet stirred reactor between simulation and experiment [75] for 1-hexene/O_2/He mixtures at an initial pressure of 10 bar (residence time = 0.5 s, 0.1% 1-hexene).

3.6 Validation Results of Iso-Hexane Skeletal Mechanism

Figure 28 shows the ignition delay time comparison between the simulation using the present mechanism and the shock tube or rapid compression machine experimental data from Zhang et al. [76] for an iso-hexane/air stoichiometric mixture at an initial pressure of 15 bar. The simulated ignition delay times using the present mechanism show very good agreements with the experimental data of both rapid compression machine and shock tube at both low-to-intermediate-temperature and intermediate-to-high-temperature conditions. To the best of the authors' knowledge for iso-hexane, fewer researchers have performed experimental studies to obtain ignition delay times at other operating conditions. The NTC (negative temperature coefficient) behavior for the rapid compression machine case is captured quite well. The reaction rate constants of the present iso-hexane skeletal mechanism are also obtained using the optimization method described in Section 2.8. Figure 29 shows the laminar flame speed comparison between the simulation from the present mechanism and the experimental data from Burluka et al. [77] for iso-hexane/air mixtures at an initial temperature of 360 K and an initial pressure of 5 bar, which is the only one dataset for iso-hexane in the literature up to now. It can be seen that the present mechanism performs well against the experimental data for equivalence ratios less than 1.2 and slightly underpredicts the experimental data for rich mixtures with equivalence ratios greater than 1.2. Figure 30 shows the comparisons of iso-hexane, O_2, CO and CO_2 concentrations in a jet stirred reactor between the simulation from the present mechanism and the experimental data from Wang et al. [78] for an iso-hexane/O_2/N_2 stoichiometric mixture at a pressure of 1.06 bar with an inlet fuel mole fraction of 2% and a residence time of 2.0 s. Overall, the experimental profiles of fuel, O_2, CO and

CO_2 can be reproduced using the present mechanism. However, the simulated profiles of fuel and O_2 are over-predicted at temperature ranges of 550~700 K and greater than 775 K.

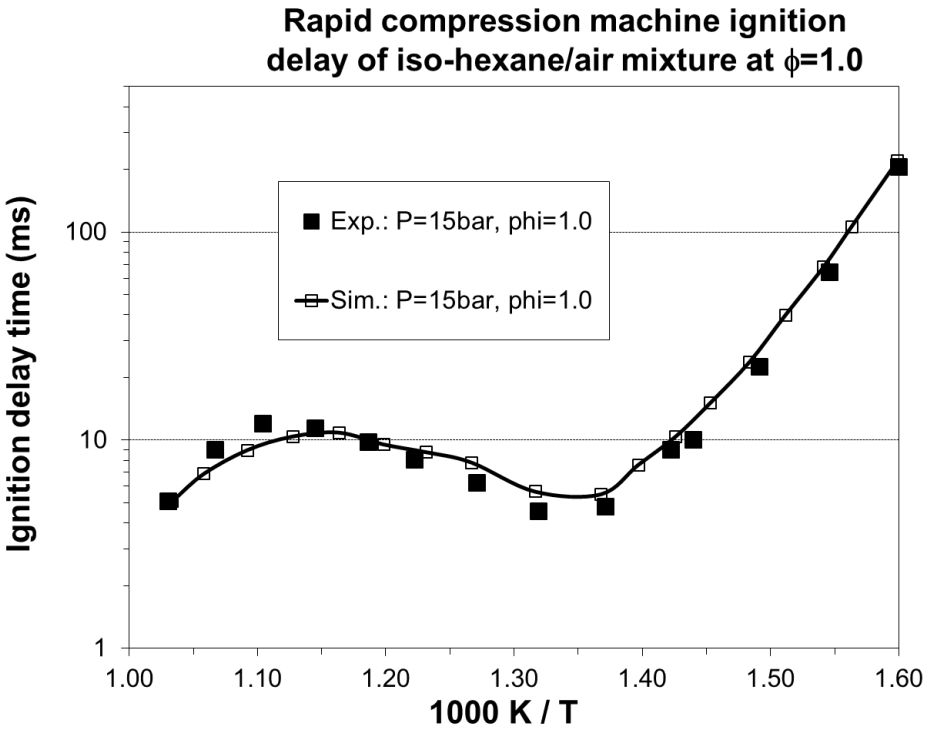

(a) rapid compression machine ignition delay.

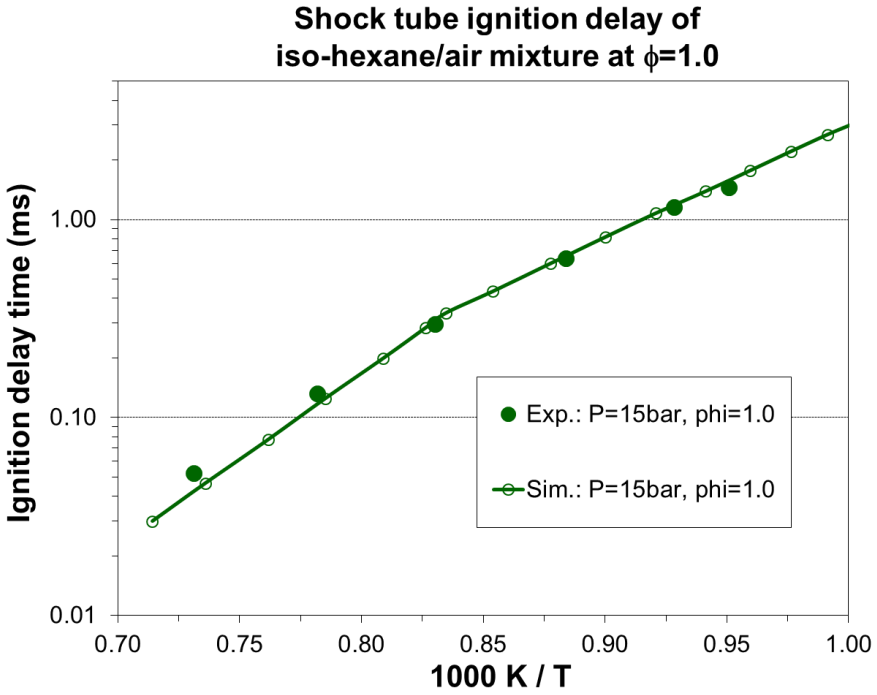

(b) shock tube ignition delay.

Figure 28. Ignition delay comparison between simulation and experiment [76] for an iso-hexane/air mixture

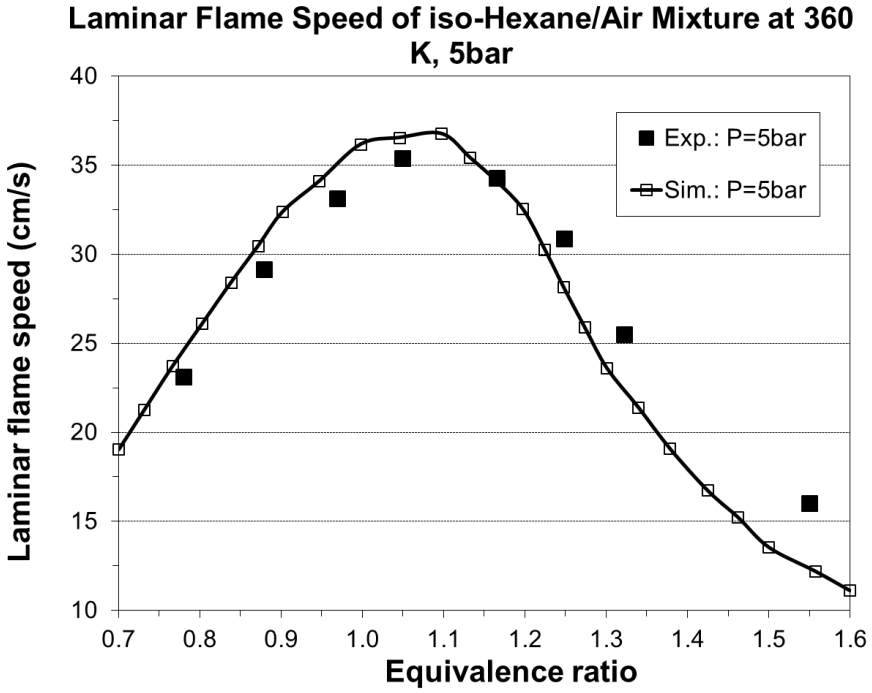

Figure 29. Laminar flame speed comparison between simulation and experiment [77] for iso-hexane/air mixtures at an initial pressure of 5 bar and an initial temperature of 360 K.

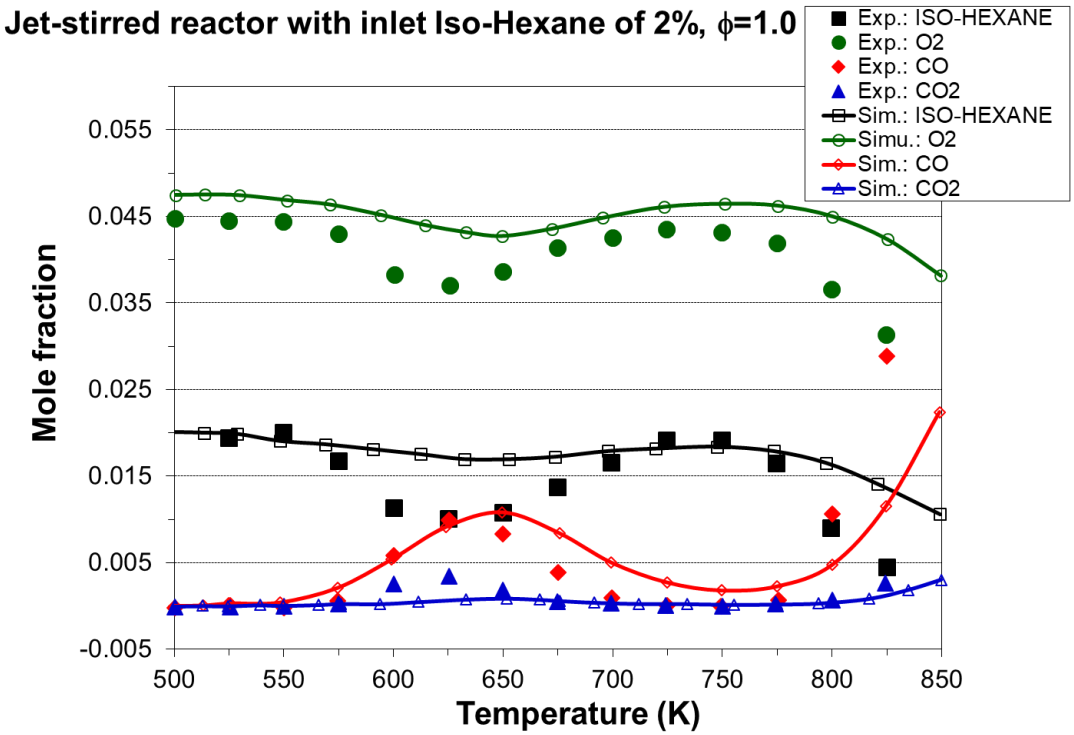

Figure 30. Comparisons of some major species concentrations in a jet stirred reactor between simulation and experiment [78] for an iso-hexane/O_2/N_2 stoichiometric mixture at an initial pressure of 1.06 bar (residence time = 2.0 s, 2.0% of inlet iso-hexane concentration).

3.7 Validation Results from Using the 5-Component Surrogate Model to Simulate Gasoline Mixtures

As mentioned in Section 3.4, the experimental gasoline/air mixtures in Figures 22 and 24 were simulated using a three-component (iso-octane, *n*-heptane, and toluene) gasoline surrogate. In this sub-Section, the 5-component gasoline surrogate model proposed in Section 2.1 is used for re-simulating the cases of Figures 22 and 24. Figure 31 shows the simulated ignition delay times using the 5-component gasoline surrogate model and comparisons with the shock tube experimental data [72] for gasoline/air mixtures. The results show that the simulated ignition delay times using the 5-component gasoline surrogate model match the experimental data quite well for all three equivalence rations. By comparing Figure 24 and Figure 31, it is seen that the worse results shown in Figure 24 for stoichiometric and rich mixtures at temperatures lower than 833 K have been greatly improved after the 5-component gasoline surrogate model was used in Figure 31.

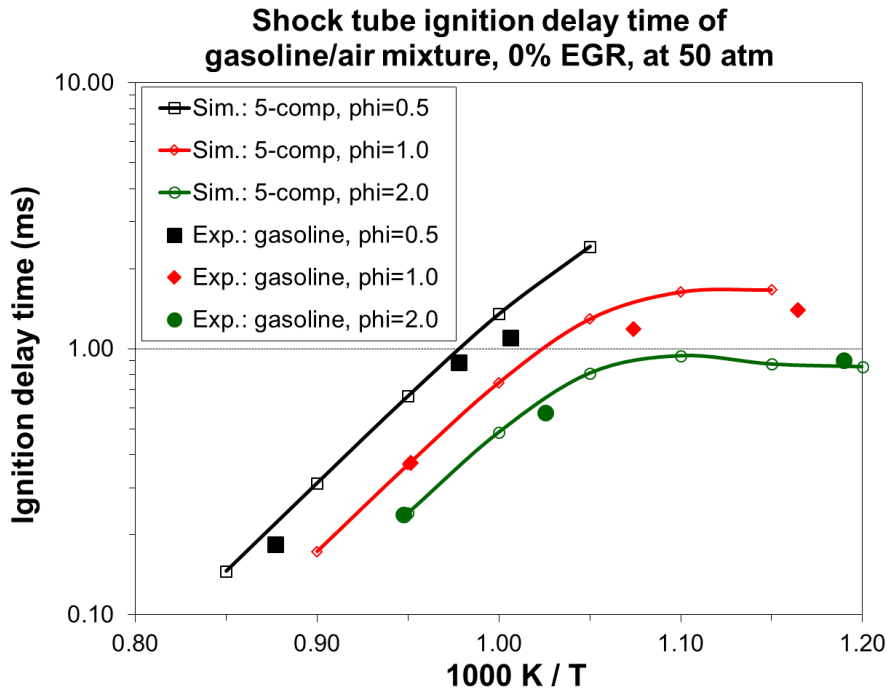

Figure 31. Simulated ignition delay times using the 5-component gasoline surrogate model and comparisons with shock tube experimental data [72] for gasoline/air mixtures.

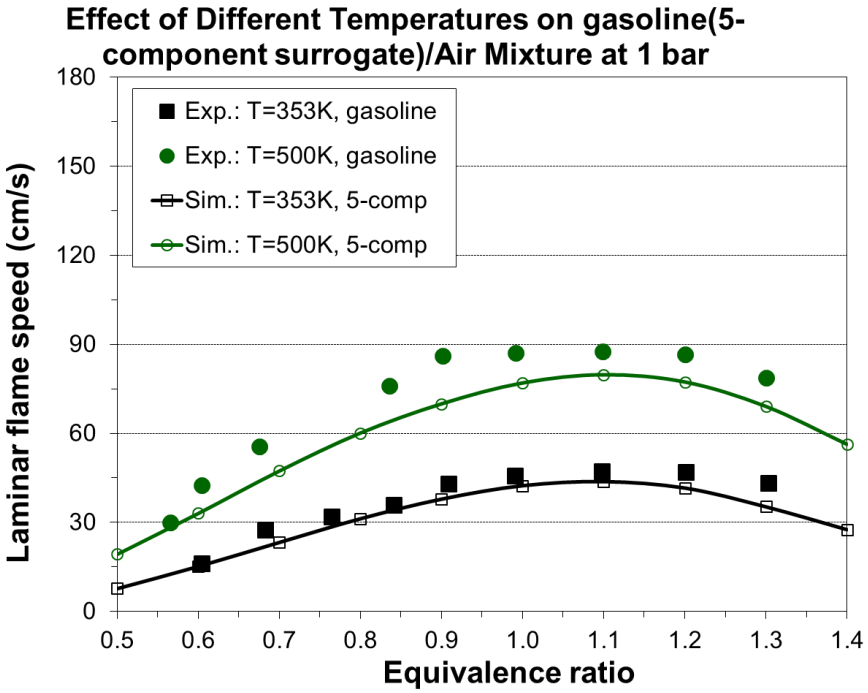

Figure 32. Simulated laminar flame speeds using the 5-component surrogate model and comparisons with experimental data [68] for gasoline/air mixtures.

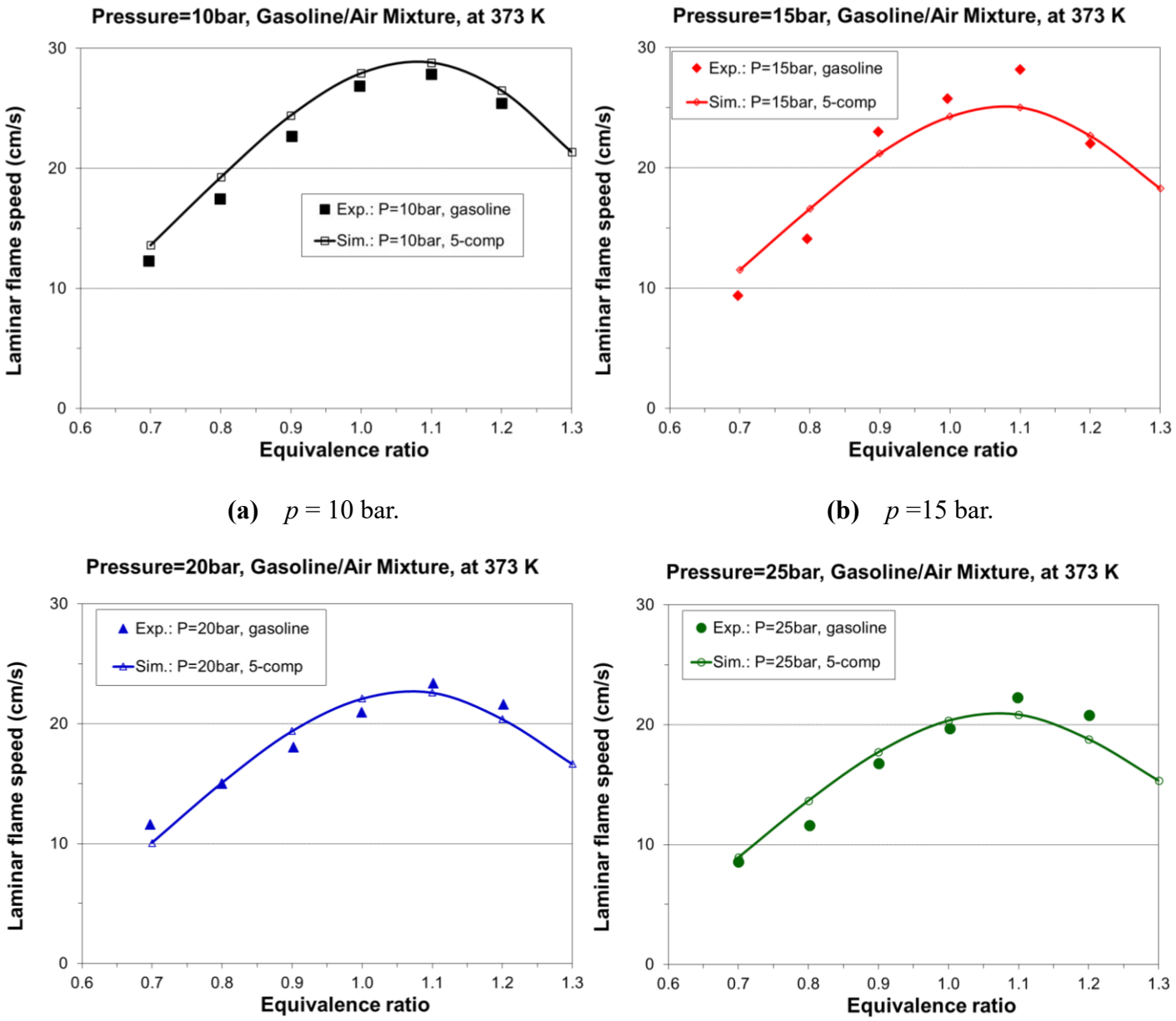

(a) p = 10 bar. **(b)** p =15 bar.

(c) p =20 bar. **(d)** p = 25 bar.

Figure 33. Simulated laminar flame speeds using the new model and comparisons with experimental data [64] for gasoline/air mixtures at an initial temperature of 373 K and various initial pressures.

Figure 32 shows the comparisons between the simulated laminar flame speeds using the 5-component gasoline surrogate model and the experimental laminar flame speeds [68] for gasoline/air mixtures at an initial pressure of 1 bar and two initial temperatures of 353 K and 500 K. The results show that the agreements

between the simulated laminar flame speeds using the 5-component gasoline surrogate model and the experimental data are quite well for the two initial temperatures. By comparing Figure 22 and Figure 32, it is seen that the underestimations shown in Figure 22 for the temperature of 500 K and for equivalence ratios greater than 1.3 under the temperature of 353 K have been improved in Figure 32 after the 5-component gasoline surrogate model was used. Also as mentioned in Section 3.3, the experimental gasoline (octane number=87)/air mixtures in Figure 16 were simulated using PRF87 (87% of iso-octane and 13% of n-heptane)/air mixtures. In this sub-Section the 5-component gasoline surrogate model mentioned above is used for re-simulating the case of Figure 16. Figure 33 shows the simulated laminar flame speeds using the new model and comparisons with the experimental data [64] for gasoline/air mixtures at an initial temperature of 373 K and four initial pressures (10 bar, 15 bar, 20 bar, and 25 bar). The results show that the new model performs quite well for the prediction of laminar flame speeds for all the four pressures from lean to rich mixtures. The much lower simulated values shown in Figure 16 for rich mixtures under the pressure of 25 bar have been greatly improved in Figure 33.

4. SUMMARY AND CONCLUSIONS

The present work presents a newly developed 5-component gasoline surrogate chemical kinetic mechanism. In the mechanism, the recently advanced $H_2/O_2/CO/C_1$ and $C_2–C_3$ detailed sub-mechanisms are adopted for predicting the laminar flame speeds accurately over a wide range of operating conditions, also five skeletal sub-mechanisms are constructed and optimized for the $C_4–C_n$ species during the oxidations of five gasoline surrogate components (iso-octane, n-heptane, iso-hexane, 1-hexene, and toluene) to simulate the ignition delay times with acceptable accuracies. The new $H_2/O_2/CO/C_1$ and $C_2–C_3$ detailed sub-mechanisms are coupled with the five $C_4–C_n$ skeletal sub-mechanisms to generate the final 5-component gasoline surrogate chemical kinetic mechanism which has 214 species and 1233 reactions including a reduced NOx sub-mechanism with 4 species and 13 reactions. The mechanism was validated extensively, including the new

$H_2/O_2/CO/C_1$ and C_2–C_3 detailed 'core' sub-mechanisms and each of the five C_4–C_n skeletal sub-mechanisms using those experimental data of ignition delay times, laminar flame speeds, and important species profiles available in the literature. Based on the model description, validation results, and analyses presented above, several conclusions can be drawn:

(1) The $H_2/O_2/CO/C_1$ and C_2–C_3 detailed sub-mechanisms have higher accuracies in terms of ignition delay times, laminar flame speeds, and major species mole fractions. The rate constants of the most important reactions in the $H_2/O_2/CO/C_1$ and C_2–C_3 detailed sub-mechanisms determined using experimentally measured values or high-level theoretically calculated values from the literature are reliable. The $H_2/O_2/CO/C_1$ and C_2–C_3 detailed sub-mechanisms can be used as the 'core' sub-mechanisms for chemical kinetic mechanism developments of other various fuels.

(2) The skeletal mechanisms with optimized reaction rate constants for the five gasoline surrogate components have very good predictions of ignition delay times, laminar flame speeds, and major species mole fractions for single component, various mixtures in the surrogate model, and real gasoline fuel under wide range of operating conditions. The final mechanism with 214 species and 1233 reactions, in which the five skeletal sub-mechanisms are coupled with the $H_2/O_2/CO/C_1$ and C_2–C_3 detailed sub-mechanisms, is feasible currently using high performance computer for simulating gasoline engine combustion, emissions, and knock.

ACKNOWLEDGMENTS

This work was partially funded by a URP (University Research Program) of Ford Motor Company. Shiyou Yang of Ford thanks Dr. Chitral Naik of Reaction Design (now ANSYS) for help in using the CHEMKIN-PRO software, also SY thanks Dr. Snehasish Panigrahy of National University of Ireland-Galway for implementing the latest propyne detailed sub-mechanism into MCCh v2.0 mechanism and providing the experimental data for validation. James Yi, Steven Wooldridge, Brad VanDerWege, Claudia Iyer, Foo-Chern Ting, and Cindy Zhou of Ford Motor Company are thanked for helpful discussions and suggestions.

REFERENCES

[1] Stanglmaier, R. and Roberts, C. Homogeneous Charge Compression Ignition (HCCI): Benefits, Compromises, and Future Engine Applications. SAE Technical Paper 1999-01-3682 (1999). DOI: 10.4271/1999-01-3682.

[2] Tamagna, D., Ra, Y., and Reitz, R. D. Multidimensional Simulation of PCCI Combustion Using Gasoline and Dual-Fuel Direct Injection with Detailed Chemical Kinetics. SAE Technical Paper 2007-01-0190 (2007). DOI: 10.4271/2007-01-0190.

[3] Kokjohn, S. L., Musculus, M., and Reitz, R. D. Evaluating Temperature and Fuel Stratification for Heat-Release Rate Control in a Reactivity-Controlled Compression-Ignition Engine Using Optical Diagnostics and Chemical Kinetics Modeling. Combustion and Flame (2015), 162(6): 2729–2742.

[4] Iwamoto, Y., Noma, K., Nakayama, O., Yamauchi, T. et al. Development of Gasoline Direct Injection Engine. SAE Technical Paper 970541 (1997). DOI: 10.4271/970541.

[5] Rose, K., Ariztegui, J., Cracknell, R., Dubois, T. et al. Exploring a Gasoline Compression Ignition (GCI) Engine Concept. SAE Technical Paper 2013-01-0911 (2013). DOI: 10.4271/2013-01-0911.

[6] Selim, H., Mohamed, S. Y., Hansen, N., and Sarathy, S. M. Premixed Flame Chemistry of a Gasoline Primary Reference Fuel Surrogate. Combustion and Flame (2017), 179(5): 300–311.

[7] Wang, H., Yao, M., Yue, Z., Jia, M., and Reitz, R. D. A Reduced Toluene Reference Fuel Chemical Kinetic Mechanism for Combustion and Polycyclic-Aromatic Hydrocarbon Predictions. Combustion and Flame (2015), 162(6): 2390–2404.

[8] Liu, X., Wang, H., Wei, L., Liu, J., and Yao, M. Development of a Reduced Toluene Reference Fuel (TRF)-2,5-Dimethylfuran-Polycyclic Aromatic Hydrocarbon (PAH) Mechanism for Engine Applications. Combustion and Flame (2016), 165(3): 453–465.

[9] Mehl, M., Pitz, W. J., Westbrook, C. K., and Curran, H. J. Kinetic Modeling of Gasoline Surrogate Components and Mixtures under Engine Conditions. Proc. Combust. Inst. (2011), 33(1): 193–200.

[10] Puduppakkam, K. V., Liang, L., Naik, C. V., Meeks, E., Kokjohn, S. L., and Reitz, R. D. Use of Detailed Kinetics and Advanced Chemistry Solution Techniques in CFD to Investigate Dual-Fuel Engine Concepts. SAE Technical Paper 2011-01-0895 (2011). DOI: 10.4271/2011-01-0895.

[11] Lu, T. and Law, C. K. A Directed Relation Graph Method for Mechanism Reduction. Proc. Combust. Inst. (2005), 30(1): 1333–1341.

[12] Pepiot-Desjardins, P. and Pitsch, H. An Efficient Error-Propagation-Based Reduction Method for Large Chemical Kinetic Mechanisms. Combustion and Flame (2008), 154(1,2): 67–81.

[13] Niemeyer, K. E. and Sung, C. Mechanism Reduction for Multicomponent Surrogates: A Case Study Using Toluene Reference Fuels. Combustion and Flame (2014), 161(11): 2752–2764.

[14] Stagni, A., Frassoldati, A., Cuoci, A., Faravelli, T., and Ranzi, E. Skeletal Mechanism Reduction through Species-Targeted Sensitivity Analysis. Combustion and Flame (2016), 163(1): 382–393.

[15] Chen, Y., Wolk, B., Mehl, M., Cheng, W. K., Chen, J. Y., and Dibble, R. W. Development of a Reduced Chemical Mechanism Targeted for a 5-Component Gasoline Surrogate: A Case Study on the Heat Release Nature in a GCI Engine. Combustion and Flame (2017), 178: 268–276.

[16] Mehl, M., Faravelli, T., Ranzi, E., Miller, D., and Cernansky, N. Experimental and Kinetic Modeling Study of the Effect of Fuel Composition in HCCI Engines. Proc. Combust. Inst. (2009), 32(2): 2843–2850.

[17] Liu, Y., Jia, M., Xie, M., and Pang, B. Improvement on a Skeletal Chemical Kinetic Model of Iso-Octane for Internal Combustion Engine by Using a Practical Methodology. Fuel (2013), 103: 884–891.

[18] Liu, Y., Jia, M., Xie, M., and Pang, B. Enhancement on a Skeletal Kinetic Model for Primary Reference Fuel Oxidation by Using a Semi-Decoupling Methodology. Energy & Fuels (2012), 26(12): 7069–7083.

[19] Yang, S., Pomraning, E., and Jia, M. Simulations of Gasoline Engine Combustion and Emissions Using a Chemical-Kinetics-Based Turbulent Premixed Combustion Modeling Approach. Proceedings of the Institution of Mechanical Engineers, Part D: Journal of Automobile Engineering (2017), 231(6): 743–765.

[20] Liu, Y., Jia, M., Xie, M., and Pang, B. Development of a New Skeletal Chemical Kinetic Model of Toluene Reference Fuel with Application to Gasoline Surrogate Fuels for Computational Fluid Dynamics Engine Simulation. Energy & Fuels (2013), 27(8): 4899–4909.

[21] Chang, Y., Jia, M., Li, Y., Liu, Y., Xie, M., Wang, H., and Reitz, R. D. Development of a Skeletal Mechanism for Diesel Surrogate Fuel by Using a Decoupling Methodology. Combustion and Flame (2015), 162: 3785–3802.

[22] Klippenstein, S. J., Harding, L. B., Davis, M. J., Tomlin, A. S., and Skodje, R. T. Uncertainty Driven Theoretical Kinetics Studies for CH_3OH Ignition: HO_2+CH_3OH and O_2+CH_3OH. Proc. Combust. Inst. (2011), 33(1): 351–357.

[23] Li, J., Zhao, Z., Kazakov, A., Chaos, M., Dryer, F. L., and Scire, Jr. J. J. A Comprehensive Kinetic Mechanism for CO, CH_2O, and CH_3OH Combustion. Int. J. Chem. Kinet. (2007), 39(3): 109–136.

[24] Patel, A., Kong, S. C., and Reitz, R. D. Development and Validation of Reduced Reaction Mechanism for HCCI Engine Simulation. SAE Technical Paper 2004-01-0558 (2004). DOI: 10.4271/2004-01-0558.

[25] Kéromnès, A., Metcalfe, W. K., Heufer, K. A., Donohoe, N., Das, A. K., Sung, C. J., Herzler, J., Naumann, C., Griebel, P., Mathieu, O., Krejci, M. C., Petersen, E. L., Pitz, W. J., and Curran, H. J. An Experimental and Detailed Chemical Kinetic Modeling Study of Hydrogen and Syngas Mixture Oxidation at Elevated Pressures. Combustion and Flame (2013), 160: 995–1011.

[26] Metcalfe, W. K., Burke, S. M., Ahmed, S. S., and Curran, H. J. A Hierarchical and Comparative Kinetic Modeling Study of C_1–C_2 Hydrocarbon and Oxygenated Fuels. Int. J. Chem. Kinet. (2013), 45(8): 638–675.

[27] Burke, U., Metcalfe, W. K., Burke, S. M., Heufer, K. A., Dagaut, P., and Curran, H. J. A Detailed Chemical Kinetic Modeling, Ignition Delay Time and Jet-Stirred Reactor Study of Methanol Oxidation. Combustion and Flame (2016), 165: 125–136.

[28] Burke, S. M., Metcalfe, W. K., Herbinet, O., Battin-Leclerc, F., Haas, F. M., Santner, J., Dryer, F. L., and Curran, H. J. An Experimental and Modeling Study of Propene Oxidation. Part 1: Speciation Measurements in Jet-Stirred and Flow Reactors. Combustion and Flame (2014), 161(11): 2765–2784.

[29] Burke, S. M., Burke, U., Mathieu, O., Osorio, I., Keesee, C., Morones, A., Petersen, E., Wang, W., DeVerter, T., Oehlschlaeger, M., Rhodes, B., Hanson, R., Davidson, D., Weber, B., Sung, C-J., Santner, J., Ju, Y., Haas, F., Dryer, F., Volkov, E., Nilsson, E., Konnov, A., Alrefae, M., Khaled, F., Farooq, A., Dirrenberger, P., Glaude, P-A., and Battin-Leclerc, F. An Experimental and Modeling Study of Propene Oxidation. Part 2: Ignition Delay Time and Flame Speed Measurements. Combustion and Flame (2015), 162(2): 296–314.

[30] Comandini, A., Dubois, T., and Chaumeix, N. Laminar Flame Speeds of n-Decane, n-Butylbenzene, and n-Propylcyclohexane Mixtures. Proc. Combust. Inst. (2015), 35(1): 671–678.

[31] Hong, Z., Davidson, D. F., Barbour, E. A., and Hanson, R. K. A New Shock Tube Study of the H + O_2 → OH + O Reaction Rate Using Tunable Diode Laser Absorption of H_2O Near 2.5 μm. Proc. Combust. Inst. (2011), 33(1): 309–316.

[32] Masten, D. A., Hanson, R. K., and Bowman, C. T. Shock Tube Study of the Reaction Hydrogen Atom + Oxygen .Fwdarw. Hydroxyl + Oxygen Atom Using Hydroxyl Laser Absorption. J. Phys. Chem. (1990), 94(18): 7119–7128.

[33] Ellingson, B. A., Theis, D. P., Tishchenko, O., Zheng, J., and Truhlar, D. G. Reactions of Hydrogen Atom with Hydrogen Peroxide. J. Phys. Chem. A (2007), 111(51): 13554–13566.

[34] Bates, R. W., Golden, D. M., Hanson, R. K., and Bowman, C. T. Experimental Study and Modeling of the Reaction H + O_2 + M → HO_2 + M (M = Ar, N_2, H_2O) at Elevated Pressures and Temperatures between 1050 and 1250 K. Phys. Chem. Chem. Phys. (2001), 3(12): 2337–2342.

[35] Fernandes, R. X., Luther, K., Troe, J., and Ushakov, V. G. Experimental and Modelling Study of the Recombination Reaction H + O_2 (+M) → HO_2 (+M) between 300 and 900 K, 1.5 and 950 bar, and in the Bath Gases M = He, Ar, and N_2. Phys. Chem. Chem. Phys. (2008), 10(29): 4313–4321.

[36] Troe, J. The Thermal Dissociation/Recombination Reaction of Hydrogen Peroxide III.: Analysis and Representation of the Temperature and Pressure Dependence over Wide Ranges. Combustion and Flame (2011), 158(4): 594–601.

[37] Lam, K.-Y., Davidson, D. F., and Hanson, R. K. A Shock Tube Study of H_2 + OH → H_2O + H Using OH Laser Absorption. Int. J. Chem. Kinet. (2013), 45(6): 363–373.

[38] Friedrichs, G., Herbon, J. T., Davidson, D. F., and Hanson, R. K. Quantitative Detection of HCO behind Shock Waves: The Thermal Decomposition of HCO. Phys. Chem. Chem. Phys. (2002), 4: 5778–5788.

[39] Timonen, R. S., Ratajczak, E., Gutman, D., and Wagner, A. F. The Addition and Dissociation Reaction Atomic Hydrogen + Carbon Monoxide .Dblharw. Oxomethyl. 2. Experimental Studies and Comparison with Theory. J. Phys. Chem. (1987), 91(20): 5325–5332.

[40] Timonen, R. S., Ratajczak, E., and Gutman, D. Kinetics of the Reactions of the Formyl Radical with Oxygen, Nitrogen Dioxide, Chlorine, and Bromine. J. Phys. Chem. (1988), 92(3): 651–655.

[41] Jasper, A. W., Klippenstein, S. J., Harding, L. B., and Ruscic, B. Kinetics of the Reaction of Methyl Radical with Hydroxyl Radical and Methanol Decomposition. J. Phys. Chem. A (2007), 111(19): 3932–3950.

[42] Smith, G. P., Golden, D. M., Frenklach, M., Moriarty, N. W., Eiteneer, B., Goldenberg, M., Bowman, C. T., Hanson, R. K., Song, S., Gardiner, W. C. Jr., Lissianski, V., and Qin, Z. Available at http://www.me.berkeley.edu/gri_mech/.

[43] Jasper, A. W., Klippenstein, S. J., and Harding, L. B. Theoretical Rate Coefficients for the Reaction of Methyl Radical with Hydroperoxyl Radical and for Methylhydroperoxide Decomposition. Proc. Combust. Inst. (2009), 32(1): 279–286.

[44] Srinivasan, N. K., Su, M. C., Sutherland, J. W., and Michael, J. V. Reflected Shock Tube Studies of High-Temperature Rate Constants for $CH_3 + O_2$, $H_2CO + O_2$, and $OH + O_2$. J. Phys. Chem. A (2005), 109(35): 7902–7914.

[45] Stewart, P. H., Larson, C. W., and Golden, D. M. Pressure and Temperature Dependence of Reactions Proceeding via a Bound Complex. 2. Application to $2CH_3 \rightarrow C_2H_5 + H^*$. Combustion and Flame (1989), 75(1): 25–31.

[46] Senosiain, J. P., Klippenstein, S. J., and Miller, J. A. Reaction of Ethylene with Hydroxyl Radicals: A Theoretical Study. J. Phys. Chem. A (2006), 110(21): 6960–6970.

[47] Aguilera-Iparraguirre, J., Curran, H. J., Klopper, W., and Simmie, J. M. Accurate Benchmark Calculation of the Reaction Barrier Height for Hydrogen Abstraction by the Hydroperoxyl Radical from Methane. Implications for C_nH_{2n+2} where $n = 2 \rightarrow 4$. J. Phys. Chem. A (2008), 112(30): 7047–7054.

[48] DeSain, J. D., Klippenstein, S. J., Miller, J. A., and Taatjes, C. A. Measurements, Theory, and Modeling of OH Formation in Ethyl + O_2 and Propyl + O_2 Reactions. J. Phys. Chem. A (2003), 107(22): 4415–4427.

[49] Panigrahy, S., Liang, J., Nagaraja, S. S., Kim, G., MacDougall, T., Vasu, S. S., and Curran, H. J. A Comprehensive Experimental and Improved Kinetic Modeling Study on the Pyrolysis and Oxidation of Propyne. Submitted to Thirty-Eighth International Symposium on Combustion (2020), July 12−17, 2020, Adelaide, Australia.

[50] Tanaka, S., Ayala, F., and Keck, J. C. A Reduced Chemical Kinetic Model for HCCI Combustion of Primary Reference Fuels in a Rapid Compression Machine. Combustion and Flame (2003), 133: 467–481.

[51] Tsurushima, T. A New Skeletal PRF Kinetic Model for HCCI Combustion. Proc. Combust. Inst. (2009), 32(2): 2835–2841.

[52] Andrae, J., Brinck, T., and Kalghatgi, G. HCCI Experiments with Toluene Reference Fuels Modeled by a Semi-Detailed Chemical Kinetic Model. Combustion and Flame (2008), 155(4): 696–712.

[53] Sakai, Y., Miyoshi, A., Koshi, M., and Pitz, W. J. A Kinetic Modeling Study on the Oxidation of Primary Reference Fuel–Toluene Mixtures Including cross Reactions between Aromatics and Aliphatics. Proc. Combust. Inst. (2009), 32(1): 411–418.

[54] Kim, Y., Min, K., Kim, M., and Chung, S. Development of a Reduced Chemical Kinetic Mechanism and Ignition Delay Measurement in a Rapid Compression Machine for CAI Combustion. SAE Technical Paper 2007-01-0218 (2007). DOI: 10.4271/2007-01-0218.

[55] Machrafi, H. and Cavadias, S. Three-Stage Autoignition of Gasoline in an HCCI Engine: An Experimental and Chemical Kinetic Modeling Investigation. Combustion and Flame (2008), 155(4): 557–570.

[56] Cai, Liming and Pitsch, Heinz. Optimized Chemical Mechanism for Combustion of Gasoline Surrogate Fuels. Combustion and Flame (2015), 162(5): 1623–1637.

[57] Cai, Liming and Pitsch, Heinz. Mechanism Optimization Based on Reaction Rate Rules. Combustion and Flame (2014), 161(2): 405–415.

[58] Ra, Y. and Reitz, R. D. A Combustion Model for IC Engine Combustion Simulations with Multi-Component Fuels. Combustion and Flame (2011), 158(1): 69-90.

[59] Zhou, C-W., Li, Y., Burke, U., Banyon, C., Somers, K. P., Khan, S., Hargis, J. W., Sikes, T., Petersen, E. L., Alabbad, M., Farooq, A., Pan, Y., Zhang, Y., Huang, Z., Lopez, J., Loparo, Z., Vasu, S. S., and Curran, H. J.

An Experimental and Chemical Kinetic Modeling Study of 1,3-Butadiene Combustion: Ignition Delay Time and Laminar Flame Speed Measurements. Combustion and Flame (2018), 197(11): 423–438.

[60] Fieweger, K., Blumenthal, R., and Adomeit, G. Self-Ignition of SI Engine Model Fuels: A Shock Tube Investigation at High Pressure. Combustion and Flame (1997), 109(4): 599–619.

[61] Kumar, K., Freeh, J. E., Sung, C. J., and Huang, Y. Laminar Flame Speeds of Preheated Iso-Octane/O_2/N_2 and N-Heptane/O_2/N_2 Mixtures. Journal of Propulsion Power (2007), 23(2): 428–436.

[62] Dagaut, P., Reuillon, M., and Cathonnet, M. High Pressure Oxidation of Liquid Fuels from Low to High Temperature. 1. N-Heptane and Iso-Octane. Combustion Science and Technology (1994), 95(1~6): 233–260.

[63] Ciezki, H. K. and Adomeit, G. Shock-Tube Investigation of Self-Ignition of N-Heptane-Air Mixtures under Engine Relevant Conditions. Combustion and Flame (1993), 93(4): 421–433.

[64] Jerzembeck, S., Peters, N., Pepiot-Desjardins, P., and Pitsch, H. Laminar Burning Velocities at High Pressure for Primary Reference Fuels and Gasoline: Experimental and Numerical Investigation. Combustion and Flame (2009), 156(2): 292–301.

[65] Dagaut, P., Reuillon, M., and Cathonnet, M. High Pressure Oxidation of Liquid Fuels from Low to High Temperature. 2. Mixtures of N-Heptane and Iso-Octane. Combustion Science and Technology (1994), 103(1~6): 315–336.

[66] Shen, H. P. S., Vanderover, J., and Oehlschlaeger, M. A. A Shock Tube Study of the Auto-Ignition of Toluene/Air Mixtures at High Pressures. Proc. Combust. Inst. (2009), 32(1): 165–172.

[67] Hartmann, M., Gushterova, I., Fikri, M., Schulz, C., Schiebl, R., and Maas, U. Auto-Ignition of Toluene-Doped N-Heptane and Iso-Octane/Air Mixtures: High-Pressure Shock-Tube Experiments and Kinetics Modeling. Combustion and Flame (2011), 158(1): 172–178.

[68] Zhao, Z., Conley, J. P., Kazakov, A., and Dryer, F. L. Burning Velocities of Real Gasoline Fuel at 353 K and 500 K. SAE Technical Paper 2003-01-3265 (2003). DOI: 10.4271/2003-01-3265.

[69] Davis, S., Wang, H., Breinsky, K., and Law, C. Laminar Flame Speeds and Oxidation Kinetics of Benene-Air and Toluene-Air Flames. Twenty-Sixth Symposium (International) on Combustion (1996), 26(1): 1025−1033, The Combustion Institute, Pittsburgh, PA.

[70] Johnston, R. J. and Farrell, J. T. Laminar Burning Velocities and Markstein Lengths of Aromatics at Elevated Temperature and Pressure. Proc. Combust. Inst. (2005), 30(1): 217–224.

[71] Moréac, G., Dagaut, P., Roesler, J., and Cathonnet, M. Nitric Oxide Interactions with Hydrocarbon Oxidation in a Jet-Stirred Reactor at 10 atm. Combustion and Flame (2006), 145(3): 512–520.

[72] Gauthier, B. M., Davidson, D. F., and Hanson, R. K. Shock Tube Determination of Ignition Delay Times in Full-Blend and Surrogate Fuel Mixtures. Combustion and Flame (2004), 139(4): 300–311.

[73] Yang, F., Deng, F., Zhang, P., Hu, E., Cheng, Y., and Huang, Z. Comparative Study on Ignition Characteristics of 1-Hexene and 2-Hexene Behind Reflected Shock Waves. Energy & Fuels (2016), 30(6): 5130–5137.

[74] Fan, X., Wang, G., Li, Y., Wang, Z., Yuan, W., and Zhao, L. Experimental and Kinetic Modeling Study of 1-Hexene Combustion at Various Pressures. Combustion and Flame (2016), 173(1): 151–160.

[75] Meng, X., Anne, R., Olivier, H., Wang, T., and Frédérique, B. Revisiting 1-Hexene Low-Temperature Oxidation. Combustion and Flame (2017), 181(7): 283–299.

[76] Zhang, K., Banyon, C., Burke, U., Kukkadapu, G., Wagnon S. W., Mehl M., Curran H. J., Westbrook C. K., and Pitz W. J. An Experimental and Kinetic Modeling Study of the Oxidation of Hexane Isomers: Developing Consistent Reaction Rate Rules for Alkanes. Combustion and Flame (2019), 206(8): 123–137.

[77] Burluka, A. A., Gaughan, R. G., Griffiths, J. F., Mandilas, C., Sheppard, C. G. W., and Woolley, R. Turbulent Burning Rates of Gasoline Components, Part 1 – Effect of Fuel Structure of C6 Hydrocarbons. Fuel (2016), 167(3): 347–356.

[78] Wang, Z., Herbinet, O., Cheng, Z., Husson, B., Fournet, R., Qi, F., and Battin-Leclerc, F. Experimental Investigation of the Low Temperature Oxidation of the Five Isomers of Hexane. J. Phys. Chem. A (2014), 118(30): 5573–5594.

NOMENCLATURE

Definitions/Abbreviations

CFD	computational fluid dynamics
CRDS	cavity-ring down spectroscopy
CVT/SCT	canonical variational transition state theory with multidimensional tunneling
DCC	dynamic cell clustering
DICI	direct injection compression ignition
DMF	dimethylfuran
DRG	direct relation graph
DRGEP	direct relation graph with error propagation
EGR	exhaust gas recirculation
GCI	gasoline compression ignition
GDI	gasoline direct injection
HCCI	homogeneous charge compression ignition
JSR	jet-stirred reactor
LHV	lower heating value
LLNL	Lawrence Livermore National Laboratory

MCCh	multi-component chemistry
MCH	methylcyclohexane
MON	motor octane number
NOx	oxides of nitrogen
NTC	negative temperature coefficient
NUI	National University of Ireland
ON	octane number
PAH	polycyclic aromatic hydrocarbon
PCCI	pre-mixed charge compression ignition
PEA	partial equilibrium approximation
PRF	primary reference fuel
QRRK	quantum Rice-Ramsperger-Kassel
QSSA	quasi steady state approximation
RCCI	reactivity controlled compression ignition
RCM	rapid compression machine
RDC	reaction during compression
RON	research octane number
ROP	rate of production
RRKM	Rice–Ramsperger–Kassel–Marcus
T50	temperature of 50% volume evaporated
TRF	toluene reference fuel
UHC	unburned hydrocarbon
URP	University Research Program

UV	ultraviolet
WWMP	world wide mapping point

Latin Symbols

D	dilution level
k_i	rate constant of reaction *i*
P	pressure
P_c	compression pressure
phi	equivalence ratio
ϕ	equivalence ratio
T	temperature
T_c	compression temperature
T_i	initial temperature
τ	ignition delay time, residence time